

## Facilitation through Buffer Saturation: Constraints on Endogenous Buffering Properties

Victor Matveev,\*<sup>†</sup> Robert S. Zucker,<sup>‡</sup> and Arthur Sherman<sup>†</sup>

\*Department of Mathematical Sciences, New Jersey Institute of Technology, Newark, New Jersey 07102; <sup>†</sup>Laboratory of Biological Modeling, National Institute of Diabetes and Digestive and Kidney Diseases, National Institutes of Health, Bethesda, Maryland 20892; and <sup>‡</sup>Molecular and Cell Biology Department, Neurobiology Division, University of California, Berkeley, California 94720

**ABSTRACT** Synaptic facilitation (SF) is a ubiquitous form of short-term plasticity, regulating synaptic dynamics on fast timescales. Although SF is known to depend on the presynaptic accumulation of  $\text{Ca}^{2+}$ , its precise mechanism is still under debate. Recently it has been shown that at certain central synapses SF results at least in part from the progressive saturation of an endogenous  $\text{Ca}^{2+}$  buffer (Blatow et al., 2003), as proposed by Klingauf and Neher (1997). Using computer simulations, we study the magnitude of SF that can be achieved by a buffer saturation mechanism (BSM), and explore its dependence on the endogenous buffering properties. We find that a high SF magnitude can be obtained either by a global saturation of a highly mobile buffer in the entire presynaptic terminal, or a local saturation of a completely immobilized buffer. A characteristic feature of BSM in both cases is that SF magnitude depends nonmonotonically on the buffer concentration. In agreement with results of Blatow et al. (2003), we find that SF grows with increasing distance from the  $\text{Ca}^{2+}$  channel cluster, and increases with increasing external  $\text{Ca}^{2+}$ ,  $[\text{Ca}^{2+}]_{\text{ext}}$ , for small levels of  $[\text{Ca}^{2+}]_{\text{ext}}$ . We compare our modeling results with the experimental properties of SF at the crayfish neuromuscular junction, and find that the saturation of an endogenous mobile buffer can explain the observed SF magnitude and its supralinear accumulation time course. However, we show that the BSM predicts slowing of the SF decay rate in the presence of exogenous  $\text{Ca}^{2+}$  buffers, contrary to experimental observations at the crayfish neuromuscular junction. Further modeling and data are required to resolve this aspect of the BSM.

### INTRODUCTION

Short-term synaptic facilitation (SF) is the transient increase of synaptic response that can be elicited by a single action potential (AP) or a short train of APs, and decays on timescales from tens to hundreds of milliseconds. It is observed in a variety of systems, from invertebrate neuromuscular junctions to neocortical synapses (reviewed in Magleby, 1987; Fisher et al., 1997; Zucker, 1994 and 1999; Zucker and Regehr, 2002). The pioneering work of Katz and Miledi (1968) and Rahamimoff (1968) showed that SF depends on the extracellular  $\text{Ca}^{2+}$ . However, there is still no agreement on the exact nature of the SF mechanism. Arguably, the simplest explanation is that SF results from the accumulation of free residual  $\text{Ca}^{2+}$  ( $[\text{Ca}^{2+}]_{\text{res}}$ ) in the presynaptic terminal. This possibility is supported by the extensive evidence that SF is sensitive to manipulations reducing the free intracellular  $\text{Ca}^{2+}$  (reviewed in Zucker and Regehr, 2002). However, early modeling work (Chad and Eckert, 1984; Simon and Llinás, 1985; Fogelson and Zucker, 1985; Roberts, 1994) demonstrated that the  $\text{Ca}^{2+}$  concentration in the vicinity of an open  $\text{Ca}^{2+}$  channel “domain” can reach very high values, from tens to hundreds of  $\mu\text{M}$ . This is much higher than the residual  $[\text{Ca}^{2+}]$  increase caused by a single AP, believed to range from 10 nM to 1  $\mu\text{M}$  (see reviews by Stanley, 1997; Neher, 1998b; Zucker, 1996 and

1999; and Zucker and Regehr, 2002). If the  $\text{Ca}^{2+}$ -dependent release machinery is located in close proximity to a  $\text{Ca}^{2+}$  channel, as suggested by the evidence of molecular interactions between the proteins mediating exocytosis and the  $\text{Ca}^{2+}$  channel proteins (reviewed in Stanley, 1997; Sheng et al., 1998; Catterall, 1999; Fisher and Bourque, 2001; Jarvis and Zamponi, 2001), it is hard to argue that such a small increase in free  $\text{Ca}^{2+}$  would lead to significant SF. Even taking into account several experimental indications that the  $\text{Ca}^{2+}$  affinity of the secretory site may be in the 5–20- $\mu\text{M}$  range rather than the 100- $\mu\text{M}$  range (Delaney and Tank, 1994; Ravin et al., 1999; Bollmann et al., 2000; Schneggenburger and Neher, 2000; Ohnuma et al., 2001), it would not be sufficient to explain the high magnitude of SF observed in many systems. One way to resolve this problem is to assume the presence of a separate high-affinity  $\text{Ca}^{2+}$ -sensitive site responsible for SF, distinct from the main secretory trigger, and located far enough from a  $\text{Ca}^{2+}$  channel, where the residual  $[\text{Ca}^{2+}]$  is comparable to the peak  $[\text{Ca}^{2+}]$  (Tang et al., 2000). We have recently shown that the properties of SF observed at the crayfish neuromuscular junction (NMJ) can be explained by such a model with two  $\text{Ca}^{2+}$ -dependent release-controlling sites, given a sufficient separation between the two sites ( $\sim 150$  nm), and under the additional assumptions of high tortuosity near the active zone and immobilization of  $\text{Ca}^{2+}$  buffers by the cytoskeleton (Matveev et al., 2002).

An alternative solution is the bound residual  $\text{Ca}^{2+}$  hypothesis, which postulates that SF results from the buildup of  $\text{Ca}^{2+}$  bound to the vesicle release sensors (Yamada and Zucker, 1992; Bertram et al., 1996; see also Bennett et al.,

Submitted September 2, 2003, and accepted for publication January 2, 2004.

Address reprint requests to Arthur Sherman, LBM, NIDDK, NIH, Bethesda, MD 20892-5621. Tel.: 301-496-4325; Fax: 301-402-0535; E-mail: asherman@nih.gov.

© 2004 by the Biophysical Society

0006-3495/04/05/2691/19 \$2.00

1997; Dittman et al., 2000). In fact, this possibility had been suggested in the pioneering studies of Katz and Miledi (1968) and Rahamimoff (1968). Within this framework, the decay time course of SF is determined by the kinetics of  $\text{Ca}^{2+}$  unbinding from the SF sensor. However, without including the effects of free  $\text{Ca}^{2+}$  in the model, this possibility is inconsistent with the above-mentioned evidence that SF is sensitive to manipulations of free intracellular  $\text{Ca}^{2+}$ .

Recently, a third, qualitatively different model of SF was put forward. It was proposed (Klingauf and Neher, 1997; Neher 1998a,b) that the fast presynaptic  $\text{Ca}^{2+}$  transients elicited by successive depolarizing pulses might themselves increase, as a result of a gradual reduction in the ability of endogenous  $\text{Ca}^{2+}$  buffers to reduce such transients, due to their progressive saturation (binding) by the residual  $\text{Ca}^{2+}$  accumulating from pulse to pulse. In this case SF would result from an increase in the size of AP-induced  $[\text{Ca}^{2+}]$  peaks, rather than an increase in free  $[\text{Ca}^{2+}]_{\text{res}}$ , or an increase in the  $\text{Ca}^{2+}$ -bound state of the release sensor (Table 1). An appealing aspect of the buffer saturation mechanism (BSM) is that it does not assume the presence of a facilitatory  $\text{Ca}^{2+}$  binding site distinct from the main secretory site, a condition required by the free residual  $\text{Ca}^{2+}$  model described above. Recently BSM has been shown to play a major role in SF at calbindin-containing neocortical and hippocampal synapses (Blatow et al., 2003), and was also inferred to contribute to SF at the calyx of Held synapse, albeit to a smaller degree (Felmy et al., 2003). The growth of  $\text{Ca}^{2+}$  transients resulting from buffer saturation has also been observed in Purkinje cells (Maeda et al., 1999) and dentate granule cell axons (Jackson and Redman, 2003). Although the buffer saturation hypothesis has been analyzed in depth by Neher (1998a) using approximate analytic methods (see also Bennett et al., 2000; Trommershäuser et al., 2003), there has yet been no rigorous systematic analysis of the conditions necessary to achieve significant SF within this framework. In this work we use computer simulations of the presynaptic spatiotemporal  $\text{Ca}^{2+}$  dynamics to study the properties of the BSM. The numerical approach allows us to consider the widest range of buffering conditions, whereas available analytic techniques rely on approximations that have limited applicability (Neher, 1998a;

Pape et al., 1998; Smith et al., 1996, 2001). Our general findings are in agreement with the experimentally observed properties of SF resulting from buffer saturation, as described by Blatow et al. (2003).

Further, we compare our modeling results with experimental recordings at the crayfish NMJ (Tang et al., 2000), to determine whether BSM could underlie the pronounced SF exhibited by this synapse. We find that the saturation of a fast mobile buffer can indeed successfully reproduce the supra-linear accumulation time course of SF, as well as the biphasic decay time course of SF observed at the crayfish NMJ. However, BSM predicts a reduction in the SF decay rate by exogenously applied buffers, whereas the opposite effect has been observed experimentally by Tang et al. (2000). We conclude that the involvement of buffer saturation in SF at the crayfish NMJ cannot be established with certainty, until more experimental data is available on  $\text{Ca}^{2+}$  homeostasis on short timescales in this preparation (see Discussion).

## METHODS

### Geometry

For simplicity, we represent the presynaptic crayfish motor bouton by a sphere 3  $\mu\text{m}$  in diameter (Fig. 1), which approximates the shape and size of real boutons (Cooper et al., 1995). The surface of the bouton is covered with active zones (AZs), with a density of 1 AZ/2.56  $\mu\text{m}^2$  (Cooper et al., 1995; Tang et al., 2000). It is assumed that all AZs are equivalent, and are distributed uniformly over the surface of the spherical bouton. This allows us to restrict our simulations to a conical region 1.8  $\mu\text{m}$  in diameter at its base, surrounding a single AZ, yielding a cone base area close to 2.56  $\mu\text{m}^2$ . We impose reflective boundary conditions for  $\text{Ca}^{2+}$  and buffer(s) on the sides of the cone, thereby assuming that the  $\text{Ca}^{2+}$  and buffer fluxes flowing into the cone from the neighboring AZ regions are balanced by the equal fluxes flowing out of the cone. This simplified geometry allows us to perform simulations in rotationally symmetric spherical ( $r, \theta$ ) coordinates, instead of solving the problem in full three dimensions. A similar method has been used by Klingauf and Neher (1997). The reduction from three to two dimensions significantly reduces the computational intensity of the simulations, allowing us to study the behavior of facilitation as two parameters are varied at a time (Figs. 3, 5, 6, 8, 9, and 13). This conical geometry is a rough approximation because the surface of a sphere cannot be tiled with disks, but the inaccuracy introduced by this simplification does not affect the qualitative features of our results.

**TABLE 1 Models of synaptic facilitation**

Model	SF site properties	SF decay mechanism	$\text{Ca}^{2+}$ buffering requirements
*Bound residual $\text{Ca}^{2+}$	Proximal, slow	$\text{Ca}^{2+}$ unbinding from SF site	No special requirements
†Free residual $\text{Ca}^{2+}$ (two-site model)	Distant, fast, high-affinity	$\text{Ca}^{2+}$ diffusion and extrusion	Immobile, high concentration
‡Buffer saturation (FCT), mobile buffer	No specialized SF site	$\text{Ca}^{2+}$ extrusion	High mobility, fast (high $k_{\text{on}}$ )
‡Buffer saturation (FCT), fixed buffer	No specialized SF site	$\text{Ca}^{2+}$ diffusion and extrusion	Low mobility, high capacity, high concentration

Endogenous  $\text{Ca}^{2+}$  buffers play a crucial role in both the residual free  $\text{Ca}^{2+}$  model and the BSM.

\*Yamada and Zucker (1992), Bertram et al. (1996); see also Regehr et al. (1994), Atluri and Regehr (1996), Bennett et al. (1997), Dittman et al. (2000).

†Tang et al. (2000), Matveev et al. (2002).

‡Klingauf and Neher (1997), Neher (1998a,b), Maeda et al. (1999), Blatow et al. (2003); see also Bennett et al. (2000), Rozov et al. (2001), Felmy et al. (2003), Jackson and Redman (2003), Trommershäuser et al. (2003).

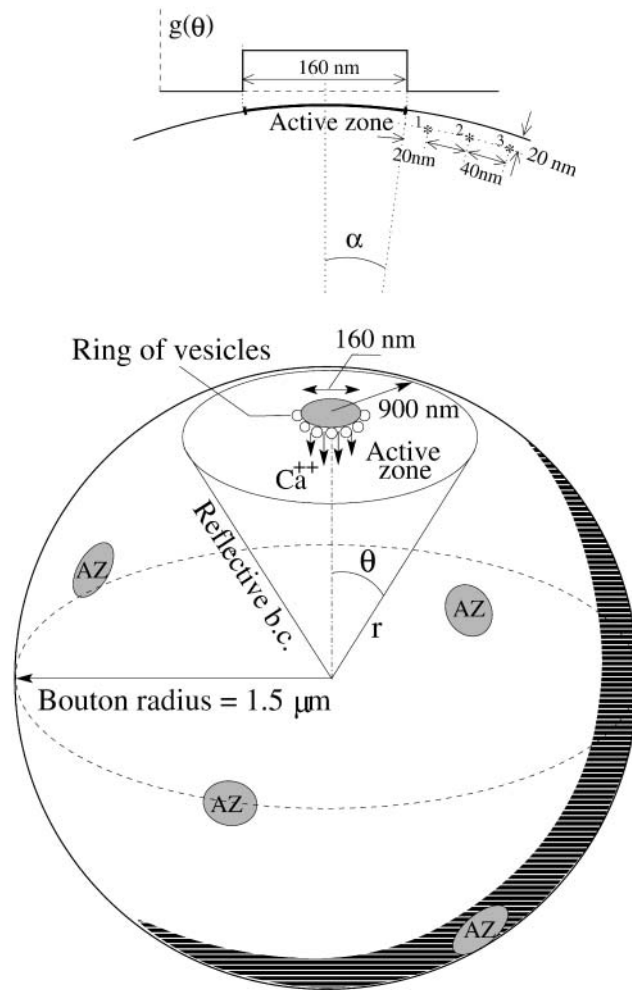


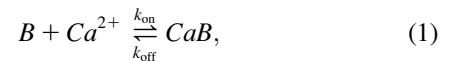
FIGURE 1 Model of a presynaptic crayfish motor bouton. The crayfish motor terminal is approximately represented as a sphere  $3 \mu\text{m}$  in diameter (bottom), with active zones (AZ) distributed evenly over the spherical surface.  $\text{Ca}^{2+}$  diffusion and buffering are only simulated in the conical region of the sphere surrounding a single AZ. The ring of vesicles around the model AZ is shown for illustration only, and is not included in the simulation. Current density  $g(\theta)$  (see Eqs. 2 and 4) is assumed to be uniformly distributed over a disk surface area  $160 \text{ nm}$  in diameter (top). Asterisks mark the locations at which the  $\text{Ca}^{2+}$  concentration is sampled during the simulations. These sites represent locations of the putative  $\text{Ca}^{2+}$  “sensors” (possible vesicle locations). We record  $\text{Ca}^{2+}$  concentration  $20 \text{ nm}$  below the membrane surface, and at lateral distances of  $20$ ,  $60$ , and  $100 \text{ nm}$  away from the edge of the  $\text{Ca}^{2+}$  current influx (corresponding sites are marked 1–3).

Ultrastructural reconstruction of the crayfish NMJ has shown that the vesicles are located around the edge of the  $\text{Ca}^{2+}$  channel cluster (Cooper et al., 1996; Atwood et al., 1997). Therefore, we are interested in the  $\text{Ca}^{2+}$  concentration achieved at the periphery of the model AZ, at different lateral distances from the edge of the channel cluster, and just below the membrane, as shown in Fig. 1 (top). The  $\text{Ca}^{2+}$  channels belonging to a single AZ are lumped together in our simulations, and the  $\text{Ca}^{2+}$  current is distributed uniformly over a disk area  $160 \text{ nm}$  in diameter (Eq. 4; Fig. 1), approximating the size of a channel cluster in a typical AZ (see Fig. 6, *Be* and *Bf*, of Atwood and Karunanithi, 2002). Vesicles themselves are not included in the simulations. The described geometry approximates the rectangular three-

dimensional geometry used in the simulations of Tang et al. (2000) and Matveev et al. (2002), with the difference that the individual  $\text{Ca}^{2+}$  channels are not resolved in the current study. Ignoring the point-like nature of  $\text{Ca}^{2+}$  influx is justified because we are not interested in an accurate description of the  $\text{Ca}^{2+}$  concentration profile in the microdomain of a single channel. As will be shown in Results, sufficient facilitation magnitude is achieved at distances of at least  $40$ – $60 \text{ nm}$  away from the edge of the cluster, which is larger than the average separation between neighboring  $\text{Ca}^{2+}$  channels. We expect the effect of the  $\text{Ca}^{2+}$  influx localization to be small at these distances, as confirmed by comparing our results with modified simulations in which  $\text{Ca}^{2+}$  influx was localized, with half entering exactly at the center and the rest entering uniformly along the edge of the AZ (i.e., the circumference of the  $160\text{-nm}$  disk). We found that the two simulations yielded nearly identical results. Thus, we are interested in what has been previously termed the “submembrane”  $\text{Ca}^{2+}$  domain (Klingauf and Neher, 1997; Bennett et al., 2000), or an AZ macrodomain. The uniformity assumption for the current distribution may also be viewed as averaging over varying positions of  $\text{Ca}^{2+}$  channels at individual AZs.

### Equations describing buffered diffusion of $\text{Ca}^{2+}$

For simplicity, in most of our simulations we assume the presence of a single dominant  $\text{Ca}^{2+}$  buffer, with the  $\text{Ca}^{2+}$  binding reaction described by



where  $k_{\text{on}}$  and  $k_{\text{off}}$  are, respectively, the binding and the unbinding rates of the  $\text{Ca}^{2+}$ -buffer compound. This leads to the following reaction-diffusion equations for the  $\text{Ca}^{2+}$  concentration,  $[\text{Ca}^{2+}]$ , and the concentration of the free (unbound) buffer,  $[B]$ :

$$\frac{\partial[\text{Ca}^{2+}]}{\partial t} = D_{\text{Ca}} \nabla^2 [\text{Ca}^{2+}] - k_{\text{on}} [\text{Ca}^{2+}] [B] + k_{\text{off}} (B_{\text{total}} - [B]) + \frac{1}{2F} I_{\text{Ca}}(t) g(\theta) \delta(r - r_b) \quad (2)$$

$$\frac{\partial[B]}{\partial t} = D_B \nabla^2 [B] - k_{\text{on}} [\text{Ca}^{2+}] [B] + k_{\text{off}} (B_{\text{total}} - [B]). \quad (3)$$

Here  $D_B$  and  $D_{\text{Ca}}$  are the diffusion coefficients in cytosol of the buffer and  $\text{Ca}^{2+}$ , respectively. We choose  $D_{\text{Ca}} = 0.2 \mu\text{m}^2 \text{ms}^{-1}$  (Allbritton et al., 1992). Following the standard convention, in Eqs. 2 and 3 we have assumed that the initial distribution of the buffer is spatially uniform, and that the diffusion coefficient of the buffer is not affected by the binding of a  $\text{Ca}^{2+}$  ion. Under these assumptions the sum of the bound and the unbound buffer concentrations is constant in space and time, and is equal to the total buffer concentration,  $B_{\text{total}}$ . This allows one to eliminate the equation for the evolution of the concentration of the bound buffer,  $[\text{CaB}] = B_{\text{total}} - [B]$ . Equations 2 and 3 are extended in a straightforward way when simulations include more than one buffer. In this case, each of the buffers evolves according to an equation identical to Eq. 3, and Eq. 2 is expanded to include the binding and the unbinding terms for each of the buffers present (e.g., see Smith et al., 2001).

The last term in Eq. 2 represents the  $\text{Ca}^{2+}$  influx, where  $F$  is Faraday’s constant,  $I_{\text{Ca}}(t)$  is the (inward) calcium current per active zone, and  $\delta(r - r_b)$  is the Dirac delta function, with  $r_b = 1.5 \mu\text{m}$  equal to the bouton radius (this describes a  $\text{Ca}^{2+}$  current flowing through the surface membrane). The surface density function  $g(\theta)$  determines the distribution of the  $\text{Ca}^{2+}$  current over the AZ surface; it is assumed to be uniform across disk surface area  $160 \text{ nm}$  in diameter ( $S_{\text{Ca}}$ ), and is zero everywhere else, as illustrated in Fig. 1 (see justification above). The integral of  $g(\theta)$  over the  $S_{\text{Ca}}$  area should be equal to one, from which we obtain

$$g(\theta) = 1/S_{Ca} = 1/(2\pi r_b^2(1 - \cos \alpha)) \sim 1/(\pi r_b^2 \alpha^2) \quad (4)$$

for  $\theta \leq \alpha$

$$g(\theta) = 0 \quad \text{for } \theta > \alpha,$$

where  $\alpha$  is the angle corresponding to the edge of the  $Ca^{2+}$  influx area:  $\alpha = 80 \text{ nm}/r_b = 0.0533 \text{ rad}$ .  $I_{Ca}(t)$  is represented as a train of simple 1-ms-long constant current pulses. Unless otherwise noted, we set  $I_{Ca}$  magnitude to 11.7 pA. This value is a factor of 2 greater than the estimate of  $I_{Ca} = 5.85 \text{ pA}$  obtained by measuring residual  $[Ca^{2+}]$  per AP (Yamada and Zucker, 1992; Tang et al., 2000), and is within the range of  $I_{Ca} = 10\text{--}50 \text{ pA}$  inferred from the measurements of  $[Ca^{2+}]$  rise rate during sustained stimulation (Tank et al., 1995; both values are translated to a 1-ms-long current pulse). In Results, we discuss the behavior of the model for variable magnitude of  $I_{Ca}$ .

Reflective boundary conditions hold for both  $[Ca^{2+}]$  and  $[B]$  at all boundaries, except for the boundary condition for  $[Ca^{2+}]$  on the top surface of the cone, which assumes  $Ca^{2+}$  extrusion by surface pumps:

$$\frac{\partial [Ca^{2+}]}{\partial r} + \frac{M}{D_{Ca}} \frac{[Ca^{2+}]}{[Ca^{2+}] + K_P} = 0. \quad (5)$$

Here  $M$  is the maximal pump rate, and  $K_P$  is the pump dissociation constant. We use values of  $K_P = 0.2 \mu\text{M}$  (Dipolo and Beauge, 1983; Carafoli, 1987) and  $M = 0.01 \mu\text{M} \mu\text{m} \text{ms}^{-1}$  (except for Fig. 12, *A* and *B*). At low  $[Ca^{2+}]$ , this yields a  $Ca^{2+}$  clearance time constant of  $\tau \sim (1 + \kappa_0) V K_P / (MS) = 5 \text{ s}$ , where  $V$  and  $S$  are the volume and the surface area of the bouton (Fig. 1), and  $\kappa_0 = 500$  is the resting state endogenous buffering capacity at the crayfish NMJ (Tank et al., 1995). This agrees with the experimental value of  $Ca^{2+}$  clearance rate obtained by Tank et al. (1995). In Results, we will discuss the possibility of higher  $Ca^{2+}$  extrusion rates. The resting buffering capacity  $\kappa_0$  (also known as the endogenous buffering ratio or the binding ratio) is an important characteristic of the buffering strength, defined as (Irving et al., 1990; Neher and Augustine, 1992)

$$\kappa_0 \equiv \left. \frac{\partial [CaB]}{\partial [Ca^{2+}]} \right|_{\text{rest}} = \frac{B_{\text{rest}}}{K_D + Ca_{\text{rest}}} = \frac{B_{\text{total}} K_D}{(K_D + Ca_{\text{rest}})^2}. \quad (6)$$

The relevant free parameters in the model are summarized in Table 2. Instead of the pair of values of  $k_{\text{off}}$  and  $k_{\text{on}}$ , we will use either  $k_{\text{on}}$  and  $K_D$  (where  $K_D = k_{\text{off}}/k_{\text{on}}$  is the dissociation constant) or  $k_{\text{off}}$  and  $K_D$  as the two independent parameters describing the buffer- $Ca^{2+}$  interaction. Note that for a fixed  $K_D$ , kinetic rates  $k_{\text{on}}$  and  $k_{\text{off}}$  are proportional to each other, so in the fixed  $K_D$  case the value of  $k_{\text{on}}$  ( $k_{\text{off}}$ ) characterizes the buffer- $Ca^{2+}$  equilibration kinetics, not just the binding (unbinding) rate. The upper bound of  $1 \mu\text{M}^{-1} \text{ms}^{-1}$  imposed on the magnitude of  $k_{\text{on}}$  is close to the theoretical diffusion limit on the maximal achievable forward binding rate for reactants with diffusion coefficients of  $0.2 \mu\text{m}^2 \text{ms}^{-1}$  (Keizer, 1987).

To further simplify the analysis, we assume that the resting  $Ca^{2+}$  concentration,  $Ca_{\text{rest}}$ , is zero. In this case the expression for the buffering capacity (Eq. 6) reduces to  $\kappa_0 = B_{\text{total}}/K_D$ . However, all our results can be

**TABLE 2 Free model parameters**

Symbol	Parameter name	Range of values
$B_{\text{total}}$	Total free buffer concentration	0–30 mM
$k_{\text{on}}$	Buffer- $Ca^{2+}$ binding rate	0.001–1 $\mu\text{M}^{-1} \text{ms}^{-1}$
$k_{\text{off}}$	Buffer- $Ca^{2+}$ unbinding rate	0.01–50 $\text{ms}^{-1}$
$D_B$	Buffer diffusion coefficient	0–0.2 $\mu\text{m}^2 \text{ms}^{-1}$
$I_{Ca}$	Calcium current per active zone	1–50 pA
$d$	Distance from the channel cluster to the SF site	20–100 nm

straightforwardly translated to the case of nonzero  $Ca_{\text{rest}}$ , as described in the Appendix. In effect, we subtract out  $Ca_{\text{rest}}$  from the total  $Ca^{2+}$  concentration and subtract the initial bound buffer concentration from  $B_{\text{total}}$ , because these are constant background values that do not affect the dynamics of  $Ca^{2+}$  diffusion. Therefore, everywhere in this paper the value of  $B_{\text{total}}$  should be understood as the initial (resting) total concentration of free buffer,  $B_{\text{rest}}$ .

## Numerical simulations

The reaction-diffusion Eqs. 2–33 were solved using the Calcium Calculator (CalC) software developed by one of us (V.M.). CalC uses an alternating-direction implicit finite-difference method, second order accurate in spatial and temporal resolution (Morton and Mayers, 1994). To preserve the accuracy of the method in the presence of the buffering term, the equations for  $[Ca^{2+}]$  and  $[B]$  are solved on separate time grids, shifted with respect to each other by half a time step (Hines, 1984). CalC uses an adaptive time-step method; the spatial grid size is adjusted to limit the error tolerance to at most 1–2% (grid of  $36 \times 36$  points in the mobile buffer case, and  $70 \times 70$  in the fixed buffer case). CalC is freely available from <http://web.njit.edu/~matveev>, and runs on Linux, SGI, and Windows/Intel platforms. To ensure reproducibility of this work, the commented simulation script files generating the data reported here will be made available on the above web site.

## RESULTS

### Facilitation of $Ca^{2+}$ transients: an example

Fig. 2 simulates the buffer saturation mechanism of SF, showing the facilitation of  $Ca^{2+}$  transients (FCT) in response to a train of five equal  $Ca^{2+}$  current steps. This growth in simulated peak  $[Ca^{2+}]$  transients is caused by the residual  $Ca^{2+}$  accumulating from pulse to pulse and gradually binding and depleting the free buffer, thereby reducing more and more the ability of the buffer to shunt the AP-triggered  $Ca^{2+}$  transients. Note that the free  $[Ca^{2+}]_{\text{res}}$  is negligibly low (see the *inset*), because most of the residual  $Ca^{2+}$  is in fact bound to the buffer, due to a high buffering ratio in our example ( $\kappa_0 = B_{\text{total}}/K_D = 1000$ ). In this and most of the following figures, concentration is shown at a distance of 60 nm from the edge of the  $Ca^{2+}$  influx region (site 2 in Fig. 1); dependence on distance will be analyzed later on (see Fig. 6).

The buffer included in the simulation is very mobile, with the diffusion coefficient of  $D_B = 0.2 \mu\text{m}^2 \text{ms}^{-1}$ , which is close to the putative mobility of ATP, for example (Naraghi and Neher, 1997). As will be shown below, strong mobility is a crucial requirement for the BSM. Because of high mobility and fast binding, the  $Ca^{2+}$  and the buffer are in equilibrium with each other and evenly distributed in space by the end of each 10-ms-long interpulse interval (data not shown). Therefore, the increase in the fifth  $Ca^{2+}$  transient,  $P_5$ , over the first  $Ca^{2+}$  transient,  $P_1$ , is completely determined by the reduction in the amount of free buffer remaining before the last pulse, denoted  $\Delta B$  ( $\Delta B = B_{\text{total}} - B_R$ ). Even at moderate values of the buffering capacity ( $\kappa_0 > 10$ ), almost all of the incoming  $Ca^{2+}$  becomes buffer-bound, so that  $\Delta B$  is approximately equal to the total (volume-averaged)  $Ca^{2+}$  influx, and therefore is solely determined by the magnitude of  $I_{Ca}$ .

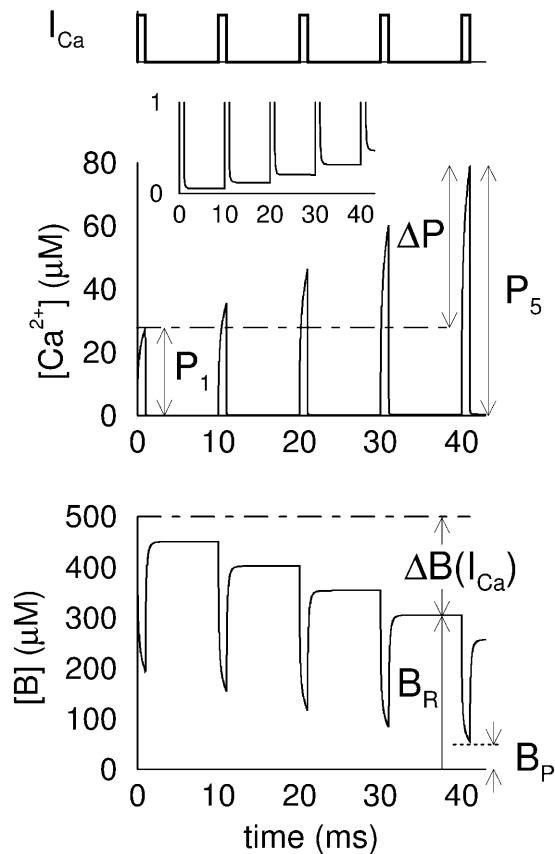


FIGURE 2 Demonstration of the facilitation of  $\text{Ca}^{2+}$  transients caused by buffer saturation.  $\text{Ca}^{2+}$  (middle panel) and buffer (bottom panel) concentration time courses produced in response to a 5-pulse train of 1-ms-long  $\text{Ca}^{2+}$  current pulses (top panel), as measured at a distance of 60 nm from the edge of the  $\text{Ca}^{2+}$  channel cluster (site 2 in Fig. 1). The growth in the  $\text{Ca}^{2+}$  transient between the fifth and the first  $\text{Ca}^{2+}$  pulses,  $\Delta P$ , depends on the degree of buffer saturation achieved right before ( $\Delta B$ ) and during ( $B_P$ ) the final pulse. See text for details. Parameters are  $B_{\text{total}} = 500 \mu\text{M}$ ,  $K_D = 0.5 \mu\text{M}$ ,  $k_{\text{on}} = 0.8 \mu\text{M}^{-1} \text{ms}^{-1}$ ,  $D_B = 0.2 \mu\text{m}^2 \text{ms}^{-1}$ , and  $I_{\text{Ca}} = 11.7 \text{ pA}$ .

### The conditions for high FCT

We will quantify FCT by the ratio of the amplitudes of the fifth and the first peaks in  $\text{Ca}^{2+}$  concentration:

$$FCT = P_5/P_1 = 1 + \Delta P/P_1. \quad (7)$$

To achieve significant FCT, one needs a large increase in the  $\text{Ca}^{2+}$  transient magnitude ( $\Delta P$ ), and a comparatively small value of the first  $\text{Ca}^{2+}$  transient,  $P_1$  (see Fig. 2). These two requirements lead to two different sets of constraints on model parameters:

1. The requirements for small  $P_1$  are straightforward and include all conditions that increase the buffering efficiency: i), large  $B_{\text{total}}$ ; ii), fast binding (large  $k_{\text{on}}$ ); iii), high buffer mobility,  $D_B$ ; iv), small  $I_{\text{Ca}}$ .
2. The conditions for large  $\Delta P$  are twofold: i), significant buffer saturation/depletion  $\Delta B$  should be achieved before

the fifth pulse; as discussed above, this requires moderately high values of  $\kappa_0$  ( $\kappa_0 > 10$ ), and high  $I_{\text{Ca}}$ ; ii), for this reduced buffer availability to make a difference, the buffer should be close to saturation during the last pulse, as well: the free buffer remaining at the end of the last pulse,  $B_P$ , should be small. In other words, initially the buffer should be effective in limiting the rise in  $\text{Ca}^{2+}$ , but at the end of the train,  $\text{Ca}^{2+}$  transients should be able to strongly saturate the buffer. This condition is easier to satisfy for low  $B_{\text{total}}$  and fast  $\text{Ca}^{2+}$ -buffer binding (high  $k_{\text{on}}$ ).

Notice that one requirement in the two groups coincides (large  $k_{\text{on}}$ ), whereas the conditions on  $B_{\text{total}}$  and  $I_{\text{Ca}}$  are in contradiction. Therefore, one may expect the FCT to grow monotonically with increasing  $k_{\text{on}}$ , but its behavior with respect to  $B_{\text{total}}$  and  $I_{\text{Ca}}$  may be nonmonotonic. The results presented below confirm this conclusion.

### FCT peaks at a finite value of $B_{\text{total}}$ , and grows monotonically with increasing $k_{\text{on}}$

Fig. 3 shows the dependence of the five-pulse FCT, defined according to Eq. 7, as a function of  $K_D$  and  $B_{\text{total}}$ , the first two model parameters in Table 2. In this figure the magnitude of the unbinding rate  $k_{\text{off}}$  is kept fixed ( $k_{\text{off}} = 0.4 \text{ ms}^{-1}$  for panel A,  $k_{\text{off}} = 0.1 \text{ ms}^{-1}$  for panel B), so the value of  $k_{\text{on}}$  varies along with the value of  $K_D$ , according to the relation  $k_{\text{on}} = k_{\text{off}}/K_D$ . The similarity between FCT values in Fig. 3, A and B, demonstrates that FCT is only weakly dependent on  $k_{\text{off}}$ , and is predominantly determined by the values of  $k_{\text{on}}$  and  $B_{\text{total}}$  (note that the range of values of  $k_{\text{on}}$ , indicated along the right margin, are equivalent in the two panels). However, the lower the value of  $k_{\text{off}}$ , the lower should be  $K_D$  to achieve a given FCT magnitude.

In agreement with the conditions formulated in the previous subsection, Fig. 3 shows that FCT grows monotonically with increasing  $k_{\text{on}}$ , but depends nonmonotonically on the value of  $B_{\text{total}}$ . For any given value of  $k_{\text{on}}$  ( $K_D$ ), maximal FCT is achieved at a certain finite value of  $B_{\text{total}}$ , which we will denote by  $B_{\text{total}}^*$  (gray curve in Fig. 3). Explaining this behavior, Fig. 4 shows the  $\text{Ca}^{2+}$  and buffer concentration time courses for three values of  $B_{\text{total}}$  that correspond to the + labels in Fig. 3 A. The middle + marks the optimal value of  $B_{\text{total}}^*$  ( $450 \mu\text{M}$ ) for  $K_D = 0.5 \mu\text{M}$  (Fig. 4 B), corresponding to the maximal FCT magnitude, whereas the two flanking values of  $B_{\text{total}}$  yield smaller values of facilitation. For  $B_{\text{total}} < B_{\text{total}}^*$  (Fig. 4 A,  $B_{\text{total}} = 200 \mu\text{M}$ ), the buffer is completely saturated during the  $\text{Ca}^{2+}$  current pulses; even though  $\Delta P$  is very large in this case, the first  $\text{Ca}^{2+}$  transient is large as well, resulting in smaller FCT compared to its value for the optimal  $B_{\text{total}} = B_{\text{total}}^*$ . In contrast, when  $B_{\text{total}} > B_{\text{total}}^*$  (Fig. 4 C,  $B_{\text{total}} = 1 \text{ mM}$ ), the buffer does not saturate to a sufficient extent, so even though the value of  $P_1$  is much reduced compared to Fig. 4, A and B, the magnitude of  $\Delta P$  is quite small, leading again to a smaller value of FCT than in the optimal ( $B_{\text{total}} = B_{\text{total}}^*$ ) case.

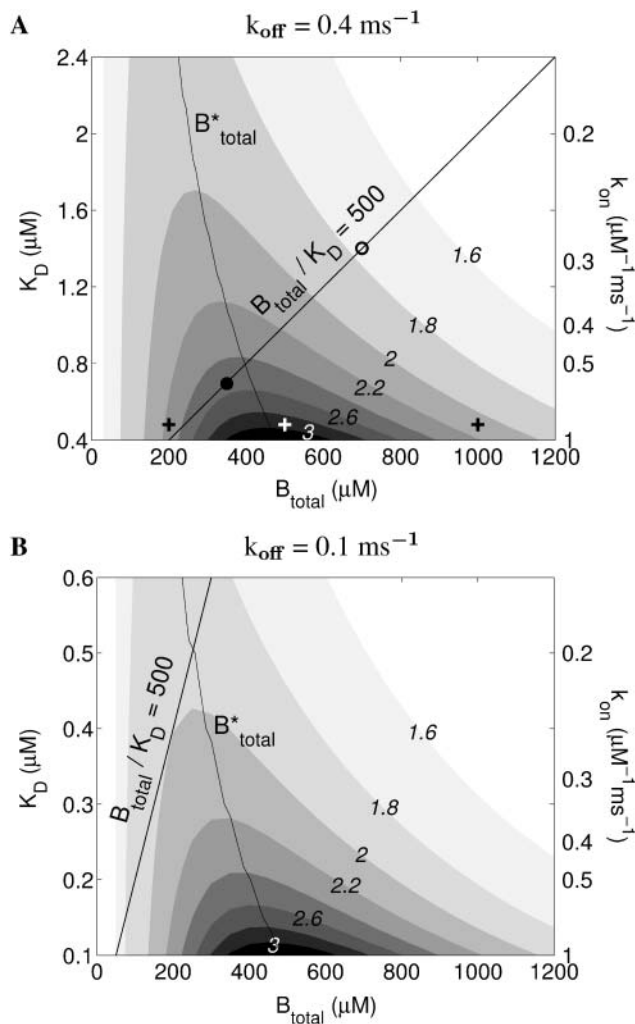


FIGURE 3 FCT as a function of buffer affinity and total buffer concentration. FCT is measured as the ratio of the fifth and the first  $\text{Ca}^{2+}$  transients,  $P_5/P_1$ , at a distance of 60 nm from the edge of the  $\text{Ca}^{2+}$  channel cluster (site 2 in Fig. 1); (A)  $k_{\text{off}} = 0.4 \text{ ms}^{-1}$  and (B)  $k_{\text{off}} = 0.1 \text{ ms}^{-1}$ . The remaining parameter values are the same as in Fig. 2 ( $D_B = 0.2 \mu\text{m}^2 \text{ms}^{-1}$ ,  $I_{\text{Ca}} = 11.7 \text{ pA}$ ). FCT is constant along the contours separating the differently shaded bands, and its value is indicated on each of the contours. FCT grows with decreasing  $K_D$  (increasing  $k_{\text{on}}$ ). Given a fixed value of  $K_D$  ( $k_{\text{on}}$ ), maximal FCT is achieved at some finite value of  $B_{\text{total}}$ , denoted  $B_{\text{total}}^*$ . (+) The parameter points corresponding to panels A–C in Fig. 4. Note the similarity between data in panels A and B, and the equal range of  $k_{\text{on}}$  values in the two cases (right scale). The diagonal line marks the set of parameter points corresponding to  $\kappa_0 = B_{\text{total}}/K_D = 500$ . Increasing (decreasing)  $I_{\text{Ca}}$  is equivalent to sliding left (right) along this line (see text for details). For example, the value of FCT for  $I_{\text{Ca}} = 5.85 \text{ pA}$ , half the value used in this plot, at the parameter point corresponding to the solid circle ( $B_{\text{total}} = 350 \mu\text{M}$ ,  $K_D = 0.7 \mu\text{M}$ ), is equal to FCT for the doubled values of  $I_{\text{Ca}}$ ,  $B_{\text{total}}$ , and  $K_D$  ( $I_{\text{Ca}} = 11.7 \text{ pA}$ ,  $B_{\text{total}} = 700 \mu\text{M}$ ,  $K_D = 1.4 \mu\text{M}$ ), corresponding to the open circle, yielding  $\text{FCT} \approx 1.8$ .

As the above analysis suggests, the optimal buffer concentration  $B_{\text{total}}^*$  should depend on the number of pulses in the stimulation train. One should expect  $B_{\text{total}}^*$  to increase with increasing train length, because more buffer is required to produce the same saturation effect for a greater total calcium

influx, which is proportional to the number of pulses. Our simulations confirm this conclusion, and show a decrease in  $B_{\text{total}}^*$  of  $\sim 10\%$  when the number of pulses is decreased from five to three (data not shown).

### FCT for a fixed value of buffering ratio

Even though the values of most of the model parameters summarized in Table 2 are not readily available from experiment, the rest-state endogenous buffering capacity,  $\kappa_0$  (see Eq. 6), can be estimated experimentally using fluorescent dye techniques (Neher and Augustine, 1992). For zero  $\text{Ca}_{\text{rest}}$ ,  $\kappa_0$  is given simply by the ratio  $B_{\text{total}}/K_D$ . We have chosen a value of 500, used in Tang et al. (2000) and Matveev et al. (2002), and close to the estimate of 600 inferred using the fluorescent  $\text{Ca}^{2+}$  sensitive dye experiments at the crayfish NMJ by Tank et al. (1995). In Fig. 3, the set of points corresponding to  $\kappa_0 = 500$  lie along the diagonal lines.

Constraining the value of  $\kappa_0$  allows us to eliminate one of the parameters from the pair  $\{K_D, B_{\text{total}}\}$ . That is, having restricted ourselves to a constant value of  $\kappa_0$  (the diagonal in Fig. 3), in Fig. 5 we can explore the dependence of FCT on an independent variation of  $k_{\text{on}}$  and  $B_{\text{total}}$  (the latter now also determines  $K_D$ , because  $B_{\text{total}} = \kappa_0 K_D$ ). In the new parameter space of Fig. 5, the locus of points corresponding to any given value of  $k_{\text{off}}$  is a hyperbolic curve. As an example, Fig. 5 A shows the two curves of points that correspond to  $k_{\text{off}} = 0.4 \text{ ms}^{-1}$  and  $k_{\text{off}} = 0.1 \text{ ms}^{-1}$ . These two hyperbolae are the images of the fixed- $\kappa_0$  diagonal lines in Fig. 3, A and B, respectively. Thus, Fig. 5 A compresses all the fixed- $\kappa_0$  information contained in a whole family of figures like Fig. 3, A and B. Moving vertically from one hyperbolic curve to the other in Fig. 5, we see that faster buffers would give greater FCT. Finally, the FCT peak in Fig. 5 A shows that the maximal magnitude of FCT is still achieved at a certain finite value of  $B_{\text{total}}$  ( $= 500 K_D$ ), even under the fixed  $\kappa_0$  constraint.

Interestingly, we find that the dependence of FCT on  $k_{\text{on}}$  and  $B_{\text{total}}$  is qualitatively as well as quantitatively similar at different values of  $\kappa_0$ . This follows from our earlier result that FCT is primarily determined by the values of  $B_{\text{total}}$  and  $k_{\text{on}}$  (Fig. 3). From the relationship  $\kappa_0 = B_{\text{total}}/K_D = (B_{\text{total}} k_{\text{on}})/k_{\text{off}}$  it is clear that increasing  $k_{\text{off}}$ , which leaves FCT almost unchanged (Fig. 3), is equivalent to a decrease in  $\kappa_0$ . Therefore, lowering the value of  $\kappa_0$ , say to  $\kappa_0 = 50$  (a 10-fold change), and simultaneously increasing  $k_{\text{off}}$  10-fold (10-fold decrease in  $K_D$ ), results only in a moderate reduction of the FCT magnitude (cf. Fig. 5, A and B).

### Dependence on $I_{\text{Ca}}$ is redundant

Apart from the value of  $\kappa_0$ , the value of  $I_{\text{Ca}}$  per action potential per AZ can also be estimated using fluorescent  $\text{Ca}^{2+}$  indicator dye measurements. However, the accuracy of

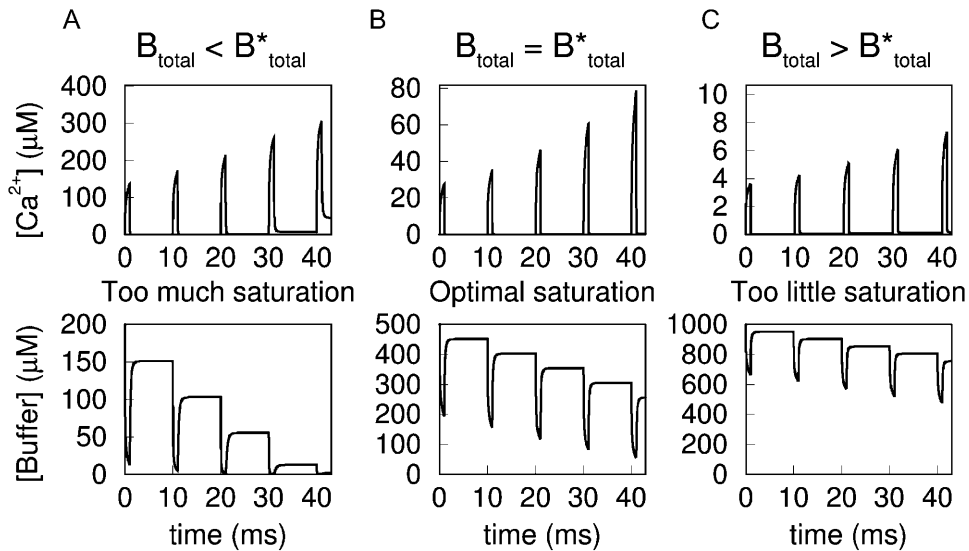


FIGURE 4 FCT in response to five  $\text{Ca}^{2+}$ -current steps, for three different values of the total buffer concentration (marked by + in Fig. 3 A). (A)  $B_{\text{total}} = 200 \mu\text{M}$ , (B)  $B_{\text{total}} = B_{\text{total}}^* = 500 \mu\text{M}$ , and (C)  $B_{\text{total}} = 1000 \mu\text{M}$ . Shown are  $[\text{Ca}^{2+}]$  (upper panels), and the buffer concentration (bottom panels) time courses. Notice the difference in scale along the concentration axis. The size of the first  $\text{Ca}^{2+}$  peak is scaled to the same level for easy comparison. FCT achieved in B is higher than in either A or C. Buffer affinity is  $K_D = 0.5 \mu\text{M}$  ( $k_{\text{on}} = 0.8 \mu\text{M}^{-1} \text{ms}^{-1}$ ), corresponding to the bottom edge of Fig. 3 A. Other parameters are the same as in Figs. 2 and 3 A ( $k_{\text{off}} = 0.4 \text{ms}^{-1}$ ,  $D_B = 0.2 \mu\text{m}^2 \text{ms}^{-1}$ ,  $I_{\text{Ca}} = 11.7 \text{pA}$ ,  $d = 60 \text{nm}$ ). Data in panel B are the same as in Fig. 2.

the  $\text{Ca}^{2+}$  influx measurements is not high, because it depends on the optical calibration of the fluorescent  $\text{Ca}^{2+}$ -sensitive dye used in the measurements, on the estimates of its concentration, and on the independent estimate of the endogenous buffering capacity,  $\kappa_0$ . Further, one may expect significant variability in  $I_{\text{Ca}}$  between different AZs, as well as between different NMJ boutons. Therefore, it is important to consider how the variation in the value of  $I_{\text{Ca}}$  would affect FCT.

As it turns out, the dependence of FCT on the magnitude of  $\text{Ca}^{2+}$  influx per AP is redundant, because knowing the dependence of FCT on  $K_D$  and  $B_{\text{total}}$ , for a given value of  $k_{\text{off}}$  (Figs. 3 and 5), gives full information about its behavior with respect to  $I_{\text{Ca}}$ . This is a consequence of the freedom in choosing the units of concentration. The FCT magnitude should not be affected if the three parameters with units of concentration,  $K_D$ ,  $B_{\text{total}}$ , and  $I_{\text{Ca}}$  (current equals concentration times volume per unit time), are rescaled by the same factor. Thus, if the FCT magnitude is calculated for a given value of the  $\text{Ca}^{2+}$  current,  $I_{\text{Ca}}$ , then at any other value of the  $\text{Ca}^{2+}$  current,  $\tilde{I}_{\text{Ca}}$ , it is given by

$$FCT(\tilde{I}_{\text{Ca}}, B_{\text{total}}, K_D; k_{\text{off}}) = FCT(I_{\text{Ca}}, a B_{\text{total}}, a K_D; k_{\text{off}}), \quad (8)$$

where  $a \equiv \tilde{I}_{\text{Ca}}/I_{\text{Ca}}$ . It follows then that changing the value of the  $\text{Ca}^{2+}$  current is equivalent to sliding along the line of constant  $B_{\text{total}}/K_D$  ratio (Figs. 3 and 5).

We have to emphasize that the above redundancy condition only holds for the FCT, and not the facilitation of neurotransmitter release. To obtain an expression similar to Eq. 8 for SF proper, given a particular choice of a  $\text{Ca}^{2+}$ -dependent exocytosis scheme, the affinity of the release mechanism to  $\text{Ca}^{2+}$  would have to be scaled along with  $I_{\text{Ca}}$ ,  $K_D$ , and  $B_{\text{total}}$  (i.e., it would have to be included in the list of

arguments that are multiplied by factor  $a$  on the right-hand side of Eq. 8). However, we assume a simple power-law relationship between release and  $[\text{Ca}^{2+}]$ , thus avoiding this complication (see ‘‘Relationship between FCT and facilitation of release’’). A similar caveat concerns the case of nonzero resting free  $[\text{Ca}^{2+}]$  value,  $\text{Ca}_{\text{rest}}$ : in general,  $\text{Ca}_{\text{rest}}$  would have to be included in the argument list on the left- and right-hand sides of Eq. 8. However, the procedure of subtracting out the  $\text{Ca}_{\text{rest}}$  value, described in the Appendix, preserves the scaling freedom expressed by Eq. 8 in the case of nonzero values of  $\text{Ca}_{\text{rest}}$  (the arguments in Eq. 8 are to be understood as the ‘‘primed’’ zero- $\text{Ca}_{\text{rest}}$  values: see Appendix). Finally, we note that the  $\text{Ca}^{2+}$  pump dissociation constant  $K_P$  (Eq. 5) constitutes yet another concentration parameter, however it mostly affects the decay time course of SF (to be discussed below), and has only moderate influence on the FCT magnitude for short-duration stimulation trains considered here.

### Relationship between FCT and facilitation of release

To compare our simulation results with the magnitude of SF available from experiment, we have to convert the FCT values into a measure characterizing facilitation of neurotransmitter release. We prefer not to constrain ourselves to a particular choice of a  $\text{Ca}^{2+}$ -dependent release model, because doing so would require introduction of additional parameters into our problem. Instead, we will assume that the synaptic response is given by the fourth power of  $[\text{Ca}^{2+}]$ . Then, SF is likewise given by the fourth power of FCT:

$$SF = \text{Facilitation}_{\text{Release}} = (\text{FCT})^4. \quad (9)$$

Note that this equation neglects the inevitable saturation of synaptic response, which would occur at sufficiently high

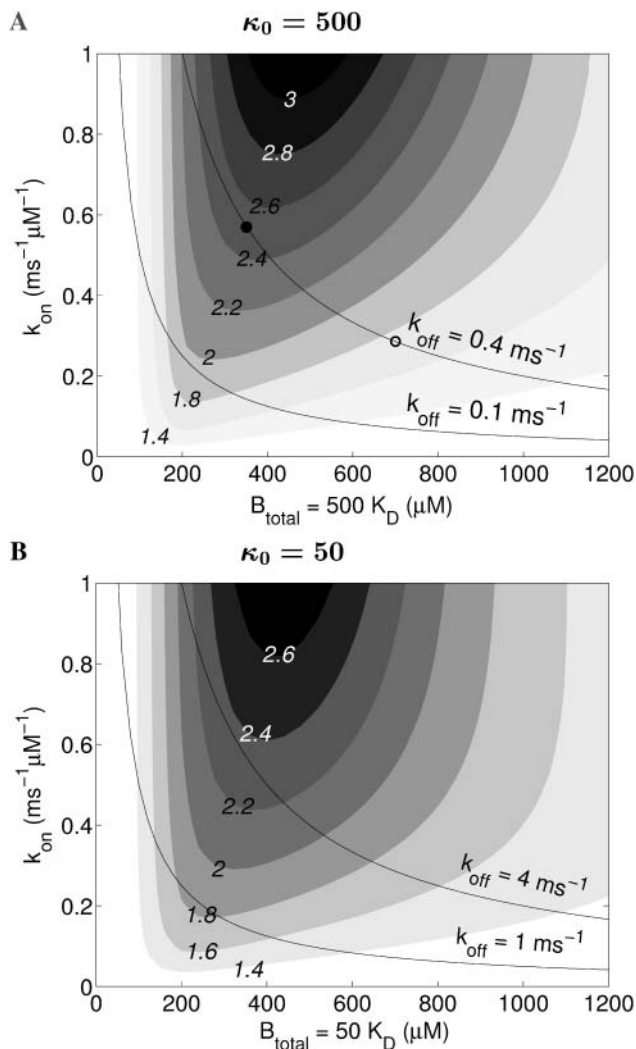


FIGURE 5 Dependence of five-pulse FCT on the values of  $k_{on}$  and  $B_{total}$  for a fixed value of the buffering ratio. (A)  $\kappa_0 = 500$ ; (B)  $\kappa_0 = 50$ . Parameter region corresponding to SF magnitude observed at the crayfish NMJ lies inside the area bounded by contour  $FCT = 2.0$  (see text for details). Hyperbolic curves mark parameter points of constant  $k_{off}$ . (A) The two curves correspond to the diagonal lines in Fig. 3, A and B. Increasing (decreasing)  $I_{Ca}$  is equivalent to sliding left (right) along these lines. Because the value of  $\kappa_0$  is fixed,  $K_D$  is determined by the value of  $B_{total}$ . Other parameters are the same as in Figs. 2–4 ( $D_B = 0.2 \mu\text{m}^2 \text{ms}^{-1}$ ,  $I_{Ca} = 11.7 \text{ pA}$ ,  $d = 60 \text{ nm}$ ).

levels of  $[\text{Ca}^{2+}]$ . Further, the cooperativity value of 4 lies at the high end of experimental range obtained for the crayfish NMJ (Landò and Zucker, 1994; Wright et al., 1996; Ravin et al., 1999; Vyshedskiy and Lin, 2000). Therefore, all facilitation estimates in this paper are to be understood as upper bounds on physiologically attainable facilitation.

Based on experimental observations, we require a five-pulse SF magnitude of  $\sim 18$ – $20$  (see Figs. 1 C and 2 C of Tang et al., 2000). This corresponds to FCT of  $P_5/P_1 \sim 2.1$  (because  $2.1^4 \sim 19.4$ ). Therefore, in the contour plots of Figs. 3 and 5, the parameter region yielding physiological

magnitude of SF lies within the area bounded by the contour of  $FCT = 2.0$ .

### FCT grows with increasing distance between $\text{Ca}^{2+}$ channel cluster and release site

There is substantial evidence for a close association between the vesicle release machinery and the presynaptic  $\text{Ca}^{2+}$  channels, suggesting their mutual proximity at many synapses (for reviews, see Stanley, 1997; Sheng et al., 1998; Catterall, 1999; Fisher and Bourque, 2001; Jarvis and Zamponi, 2001). At the crayfish NMJ, morphological studies suggest that vesicles are clustered along the edge of the AZ (Cooper et al., 1996; Atwood et al., 1997; Atwood and Karunanithi, 2002). However, at certain synapses, like the calyx of Held, vesicles may be scattered at various distances from the  $\text{Ca}^{2+}$  channel cluster (Meinrenken et al., 2002; Sätzler et al., 2002). Further, recent experiments on the sensitivity of phasic response to an application of a fast exogenous buffer (1,2-bis(2-aminophenoxy)ethane-*N,N,N',N'*-tetraacetic acid (BAPTA)) suggest that there is a significant separation between  $\text{Ca}^{2+}$  channels and secretion triggers at several strongly facilitating, but not at depressing, neocortical and hippocampal synapses (Rozov et al., 2001; Blatow et al., 2003). For any synapse type, it is possible that various obstacles to diffusion (such as vesicles themselves) and the tortuosity effects associated with the dense cytoskeletal and protein mesh within the AZ may significantly increase the effective diffusional distance between the  $\text{Ca}^{2+}$  channel and the release-triggering  $\text{Ca}^{2+}$  sensor. Therefore, we simulated the  $\text{Ca}^{2+}$  transients at various distances from the  $\text{Ca}^{2+}$  influx region. Fig. 6 A demonstrates that the magnitude of FCT is increased by an increase in the channel-sensor separation. This result is easy to understand, because the buffer is able to bind more  $\text{Ca}^{2+}$  when it is acting over a longer diffusional distance (see review by Neher, 1998b), and thereby is more effective in reducing the first response,  $P_1$ , leading to higher FCT. Sufficient SF is achieved at distances of at least 40–60 nm from the  $\text{Ca}^{2+}$  channel cluster.

### Facilitation growth is supralinear

As discussed above, Figs. 5 and 6 A demonstrate that the physiological magnitude of five-pulse SF can be achieved within a certain range of values of  $k_{on}$  and  $B_{total}$  ( $K_D$ ). However, we also need to establish whether BSM can reproduce the supralinear accumulation time course of SF observed at the crayfish NMJ (Figs. 1 C and 2 C of Tang et al., 2000; Fig. 2 C of Winslow et al., 1994). Traces in Fig. 6 B show that the simulated growth of FCT for a chosen parameter point (marked by an *asterisk* in Fig. 6 A) is indeed supralinear, at all distances from the  $\text{Ca}^{2+}$  channel cluster, and therefore facilitation of release (Eq. 9) grows supralinearly as well, in agreement with experiment. Fig. 7 A demonstrates the supralinear time course of SF corresponding to the  $[\text{Ca}^{2+}]$



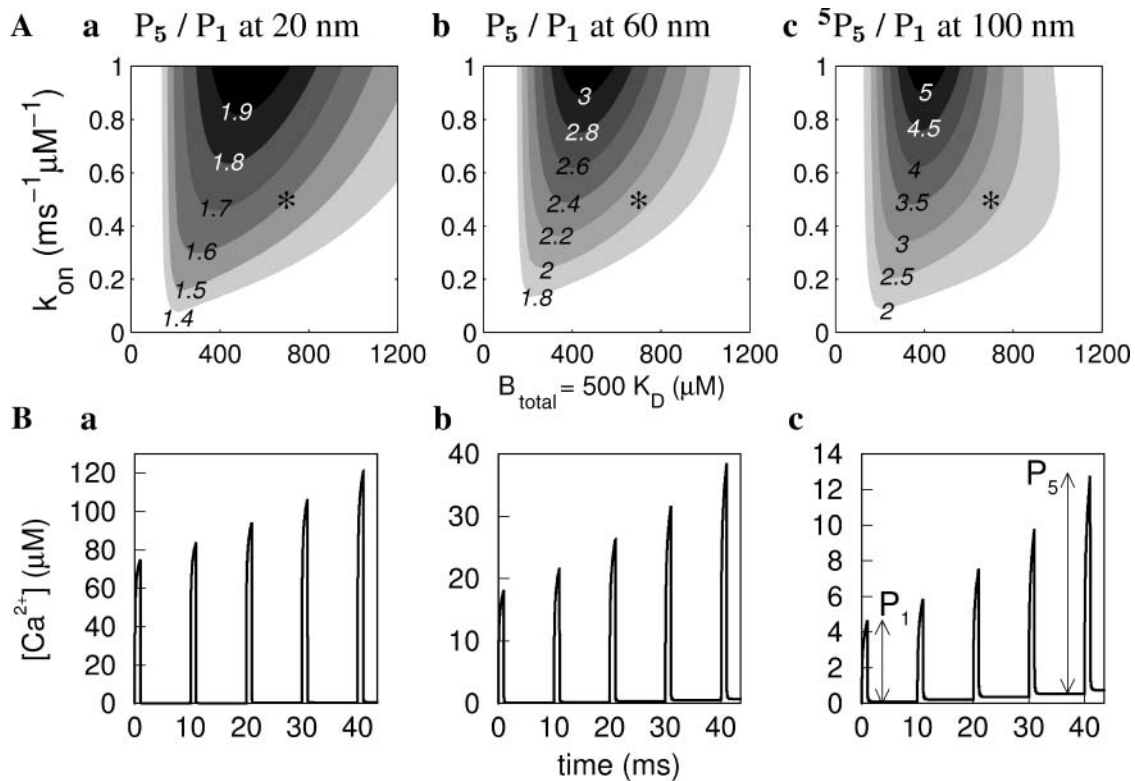


FIGURE 6 FCT increases with increasing distance from the  $\text{Ca}^{2+}$  channel cluster. (A) Five-pulse FCT as a function of  $B_{\text{total}}$  and  $k_{\text{on}}$ , at distances of (a) 20 nm, (b) 60 nm, and (c) 100 nm away from the edge of the channel cluster (locations marked 1–3 in Fig. 1). Data in panel Ab are the same as in Fig. 5 A. (B)  $[\text{Ca}^{2+}]$  time course for parameter values corresponding to the points marked with an asterisk in A ( $B_{\text{total}} = 700 \mu\text{M}$ ,  $K_D = 1.4 \mu\text{M}$ ,  $k_{\text{on}} = 0.5 \mu\text{M}^{-1} \text{ms}^{-1}$ ). Note the difference in scale along the concentration axis. Other parameter values are the same as in Figs. 2–5 ( $D_B = 0.2 \mu\text{m}^2 \text{ms}^{-1}$ ,  $I_{\text{Ca}} = 11.7 \text{ pA}$ ).

trace shown Fig. 6 Bb, yielding a physiological SF magnitude. In fact, we find that, for a mobile buffer, the parameter region yielding high facilitation coincides with the region of high supralinearity (data not shown). Therefore, BSM can successfully reproduce the SF magnitude and its accumulation time course observed experimentally at the crayfish NMJ.

### Effect of exogenous buffers on facilitation growth

The experimental observations of the reduction of SF by exogenously applied buffers were crucial for establishing the role of residual  $\text{Ca}^{2+}$  in SF (see review by Zucker and Regehr, 2002), and a successful SF model should reproduce this property. Fig. 7 A shows the simulated effect of application of  $200 \mu\text{M}$  of Fura-2, a fast and high-affinity mobile buffer, on SF magnitude, for a set of parameter values marked by an asterisk in Fig. 6 Ab. These simulation results agree very well with the experimental results of Tang et al. (2000) (Fig. 7 B). However, due to the nonmonotonic dependence of FCT on  $B_{\text{total}}$ , adding a mobile high-affinity buffer may actually increase FCT, and hence SF, under certain conditions. Such paradoxical effect of exogenous buffers on SF has been termed “pseudofacilitation” (Neher, 1998a; Rozov et al., 2001; Blatow et al., 2003; see also Discussion).

### FCT at lower buffer mobility

Until now we have assumed that the  $\text{Ca}^{2+}$  buffer is highly mobile, with a diffusion coefficient comparable to that of ATP, BAPTA, or EGTA (Naraghi and Neher, 1997). There are several studies that agree with such high mobility of endogenous buffers, for instance the experiments at goldfish retinal bipolar cells (Burrone et al., 2002), Purkinje cells (Maeda et al., 1999), and frog saccular hair cells (Roberts, 1993). However, endogenous buffers were found to be immobile or poorly mobile in many other preparations, including the calyx of Held (Helmchen et al., 1997), neocortical, and hippocampal pyramidal cells (Helmchen et al., 1996; Ohana and Sakmann, 1998; Lee et al., 2000), axons of Aplysia neurons (Gabso et al., 1997), and bovine adrenal chromaffin cells (Neher and Augustine, 1992; Zhou and Neher, 1993; Xu et al., 1997). At the crayfish NMJ, the mobility of endogenous  $\text{Ca}^{2+}$  buffers is not known. To study the dependence of the BSM on buffer mobility, we repeated our simulations for variable values of  $B_{\text{total}}$  and the  $D_B$ , the only parameter in Table 2 yet to be varied, for fixed values of  $\kappa_0$  and  $k_{\text{on}}$  ( $\kappa_0 = 500$ ,  $k_{\text{on}} = 0.8 \mu\text{M}^{-1} \text{ms}^{-1}$ ). Fig. 8 A shows that FCT declines dramatically as  $D_B$  is decreased, which agrees with the conditions for high FCT that were formulated in the section entitled “Facilitation of  $\text{Ca}^{2+}$  transients: an

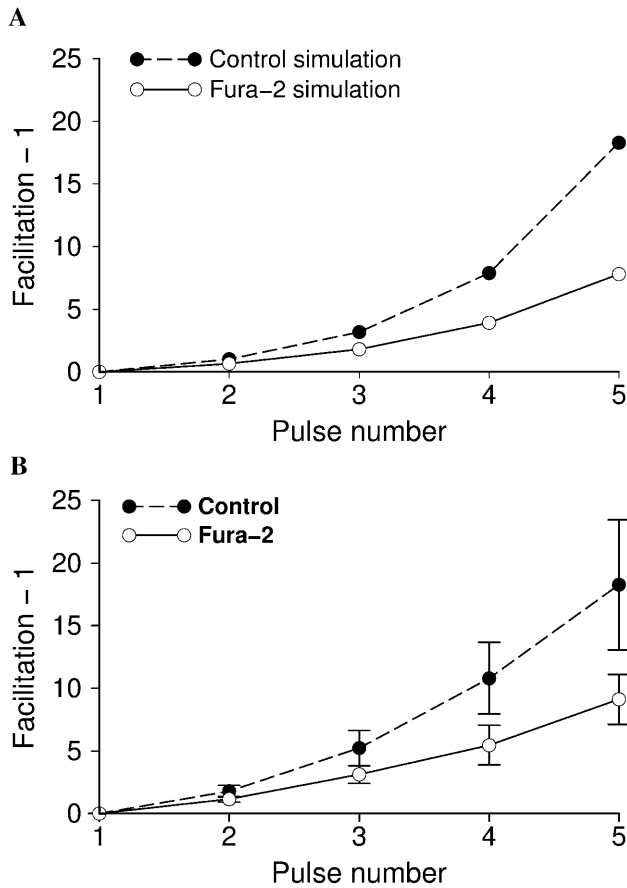


FIGURE 7 Facilitation grows supralinearly in the mobile buffer case. Comparison of (A) simulation results with (B) experimental data from Fig. 3 C of Tang et al. (2000), showing SF for a five-pulse 100-Hz train, with and without Fura-2. In A, simulations are performed for parameter values corresponding to the point marked by an asterisk in Fig. 6 Ab (distance = 60 nm,  $B_{\text{total}} = 700 \mu\text{M}$ ,  $K_D = 1.4 \mu\text{M}$ ,  $k_{\text{on}} = 0.5 \mu\text{M}^{-1} \text{ms}^{-1}$ ,  $D_B = 0.2 \mu\text{m}^2 \text{ms}^{-1}$ ,  $I_{\text{Ca}} = 11.7 \text{pA}$ ). Facilitation is normalized to zero for the first pulse:  $([\text{Ca}^{2+}]^n/[\text{Ca}^{2+}]^1)^4 - 1$  (Eqs. 11 and 12). The  $[\text{Ca}^{2+}]$  trace corresponding to the control simulation curve in A is shown in Fig. 6 Bb. The following parameter values are used for the Fura-2 in A:  $B_{\text{total}} = 200 \mu\text{M}$ ,  $K_D = 360 \text{nM}$ ,  $k_{\text{on}} = 0.27 \mu\text{M}^{-1} \text{ms}^{-1}$ , and  $D_B = 0.118 \mu\text{m}^2 \text{ms}^{-1}$  (Tang et al., 2000).

example.” At the same time, there is an increase in the optimal buffer concentration required to achieve maximal FCT. This is because a buffer with lower mobility is saturated much more readily, so greater  $B_{\text{total}}$  is required to prevent oversaturation. However, we find that the transition to the fixed buffer case ( $D_B = 0$ ) is nonmonotonic, and FCT starts increasing as  $D_B$  drops below  $\sim 0.01 \mu\text{m}^2 \text{ms}^{-1}$  (Fig. 8 B), suggesting the existence of a distinct facilitation regime at very low values of  $D_B$ .

### FCT in the fixed buffer case

At low mobility and high  $B_{\text{total}}$  it becomes possible for the buffer to absorb most of the  $\text{Ca}^{2+}$  influx before it reaches the

$\text{Ca}^{2+}$  sensor, strongly decreasing the first few responses, and thereby leading to a high FCT magnitude. This regime is most pronounced when the buffer is completely immobile; as Fig. 8 B shows, FCT rapidly decreases even for small nonzero values of  $D_B$ . Fig. 9 A illustrates the behavior of FCT for  $D_B = 0$ , as a function of  $k_{\text{on}}$  and  $B_{\text{total}}$  ( $= 500 K_D$ ), at different distances from the  $\text{Ca}^{2+}$  channel cluster (compare with the mobile buffer case, Fig. 6). FCT is seen to be relatively weakly dependent on  $k_{\text{on}}$ , for sufficiently high values of  $k_{\text{on}}$ . This is because the effective diffusional distance from the point of influx to the  $\text{Ca}^{2+}$  sensor is significantly increased in the presence of a fixed buffer, assuring that the  $\text{Ca}^{2+}$  ions will undergo multiple binding-unbinding steps for a wide range of  $k_{\text{on}}$  values. For this reason, FCT is sensitive to the buffer affinity,  $K_D$ , and not to  $k_{\text{on}}$ , as in the mobile buffer case. Therefore, FCT is also sensitive to the value of buffering capacity,  $\kappa_0$ . We find that large  $\kappa_0$  is required to achieve high FCT in the fixed buffer case (data not shown).

The  $[\text{Ca}^{2+}]_{\text{res}}$  traces shown in Fig. 9 B demonstrate that the free  $[\text{Ca}^{2+}]_{\text{res}}$  makes a more significant contribution to  $\text{Ca}^{2+}$  peaks, as compared to the case of a mobile buffer (cf. Fig. 6 B). In fact, we find that the regions of high FCT and high free  $[\text{Ca}^{2+}]_{\text{res}}$  significantly overlap (data not shown). When  $[\text{Ca}^{2+}]_{\text{res}}$  is nonnegligible, Eq. 9 should be modified to include its contribution to facilitation:

$$\begin{aligned} \text{Facilitation}_{\text{Release}} &= ((P_5 + R_4)/P_1)^4 \\ &= (\text{FCT} + R_4/P_1)^4, \end{aligned} \quad (10)$$

where  $R_4$  equals  $[\text{Ca}^{2+}]_{\text{res}}$  achieved at the end of the fourth interpulse interval (see Fig. 9 Bb). The  $R_4/P_1$  ratio should remain much smaller than one, because the delayed asynchronous release 10 ms after the fourth pulse is known to be much smaller than the peak synaptic response achieved during the first pulse. The contribution of  $[\text{Ca}^{2+}]_{\text{res}}$  increases with increasing  $B_{\text{total}}$  ( $K_D$ ), and with increasing distance from the  $\text{Ca}^{2+}$  channel cluster. In fact, for sufficiently high  $B_{\text{total}}$  values and at large distances, the fast  $\text{Ca}^{2+}$  transient becomes completely shunted by the buffer, and the peak in  $\text{Ca}^{2+}$  concentration is significantly delayed with respect to the end of the pulse (in Fig. 9 Bc, the delay is 1.5 ms). Under these conditions the BSM would predict a physiologically unrealistic latency between the end of the  $\text{Ca}^{2+}$  influx and the peak of neurotransmitter release. At a given distance, there is only a narrow range of  $B_{\text{total}}$  values where the magnitude of facilitation (Eq. 10) reaches experimentally observed levels, whereas the free  $[\text{Ca}^{2+}]_{\text{res}}$  contribution remains small ( $R_4/P_1 \leq 0.2$ ). For a distance of 60 nm (Fig. 9 Ab), the corresponding range is  $\sim 10$ – $12 \text{mM}$ , approaching unphysiologically high concentrations.

Fig. 10 demonstrates the spatial distribution of the  $\text{Ca}^{2+}$  ions and the buffer at different times after the cessation of an AP, for a parameter point marked with a + in Fig. 9 A. Contrary to the mobile buffer case, it takes tens of

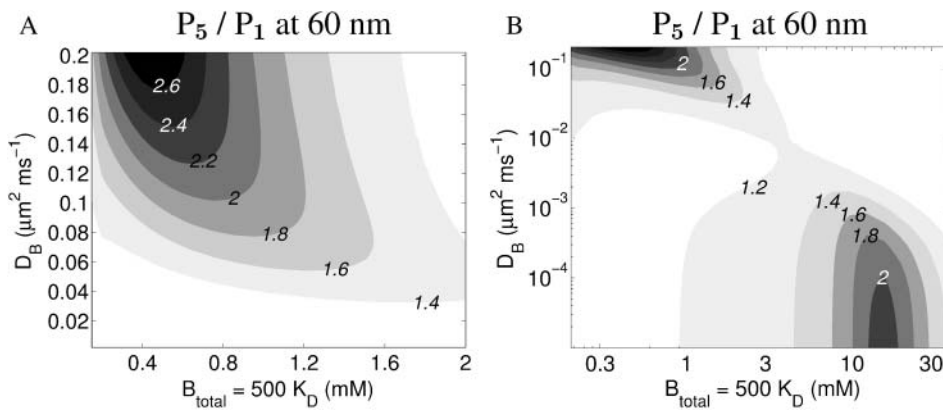


FIGURE 8 Dependence of FCT on buffer mobility. Shown is the five-pulse FCT as a function of the buffer diffusion coefficient,  $D_B$ , and  $B_{\text{total}}$  ( $K_D$ ), for  $\kappa_0 = 500$ . Panel *B* extends the data in panel *A* into the region of very high  $B_{\text{total}}$ , and uses logarithmic scale to emphasize the region of very small  $D_B$ . Note the two FCT peaks, one at large  $D_B$  and small  $B_{\text{total}}$ , and another peak at  $D_B$  close to zero and very large  $B_{\text{total}}$ . Parameter values are  $k_{\text{on}} = 0.8 \mu\text{M}^{-1} \text{ms}^{-1}$ ,  $I_{\text{Ca}} = 11.7 \text{ pA}$ , and  $d = 60 \text{ nm}$ . The set of points along the top edge of all panels ( $D_B = 0.2 \mu\text{m}^2 \text{ms}^{-1}$ ) correspond to the horizontal line  $k_{\text{on}} = 0.8 \mu\text{M}^{-1} \text{ms}^{-1}$  in Figs. 5 and 6 *Ab*).

milliseconds rather than a fraction of one millisecond for the concentrations to reequilibrate in space, so the free  $[\text{Ca}^{2+}]_{\text{res}}$  elevation and the buffer saturation region are still significantly localized by the end of a 10-ms-long interpulse interval. This illustrates that it is a local rather than global buffer saturation that underlies FCT in the fixed buffer case.

Further, we find that the accumulation time course of SF is sublinear for a fixed buffer. Fig. 9 *Bb* shows the  $[\text{Ca}^{2+}]$  trace, and Fig. 11 depicts the corresponding SF growth time course at a distance of 60 nm from the edge of the  $\text{Ca}^{2+}$  influx region, for a parameter point marked with a + in Fig. 9 *Ab*.

In fact, we find that the SF accumulation time course remains sublinear for any choice of parameter values (data not shown).

### Facilitation decay time course and the effect of Fura-2 on facilitation decay

Above we have shown that high buffer mobility is important for the BSM to explain the experimentally observed supralinear accumulation time course of SF. For a highly mobile buffer, the  $\text{Ca}^{2+}$  concentration rapidly reequilibrates

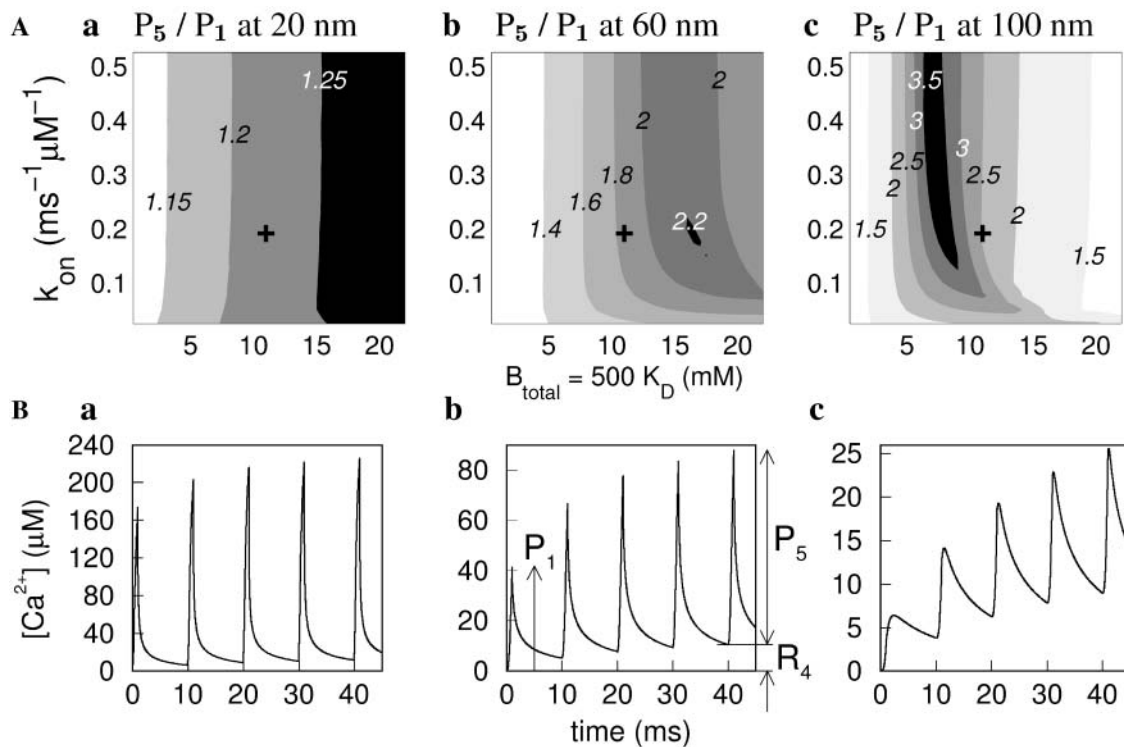


FIGURE 9 FCT as a function of  $B_{\text{total}}$  and  $k_{\text{on}}$  in the fixed buffer case, for a constant value of the buffering capacity,  $\kappa_0 = 500$ . This is the same as Fig. 6, except that  $D_B = 0$ . Note that much higher  $B_{\text{total}}$  is required to achieve significant facilitation, and the slower decay of the  $\text{Ca}^{2+}$  transients, as compared to the mobile buffer case (cf. Fig. 6).

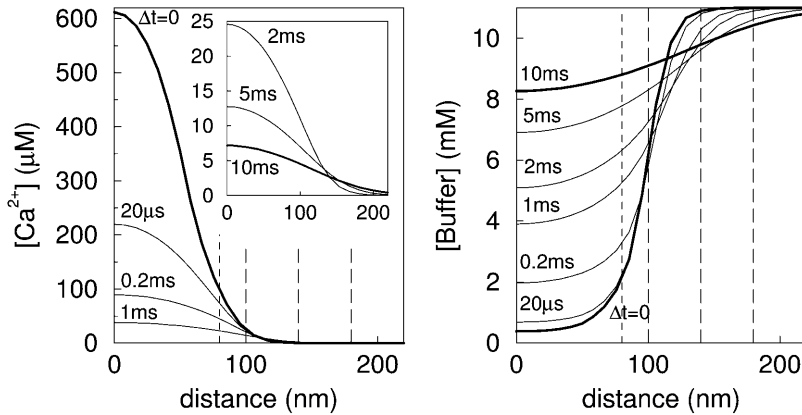


FIGURE 10 Slow spatial reequilibration of  $\text{Ca}^{2+}$  and fixed buffer after an action potential. Panels on the left (right) demonstrate the  $\text{Ca}^{2+}$  (buffer) concentration profiles, respectively, at different times (indicated on the corresponding contours) after the cessation of a 1-ms-long  $\text{Ca}^{2+}$  current pulse. The profiles are shown along an axis situated 20 nm below the synaptic membrane, and running parallel to it (dotted line in Fig. 2). The inset shows  $[\text{Ca}^{2+}]$  profiles on a finer concentration scale, at later times. The short-dashed vertical line marks the edge of the  $\text{Ca}^{2+}$  influx region (distance of 80 nm), whereas the long-dashed lines correspond to the three sites marked by asterisks in Fig. 1 (distances of 100 nm, 140 nm, and 180 nm from the AZ center, or 20 nm, 60 nm, and 100 nm from the edge of the influx region). Parameter values correspond to a point marked by a + in Fig. 9 A. At the end of the 10-ms-long interpulse interval, there is still a significant nonuniform (localized) saturation of the fixed buffer, which is in equilibrium with the locally elevated residual free  $\text{Ca}^{2+}$  (inset).

throughout the terminal upon termination of the  $\text{Ca}^{2+}$  influx caused by an AP. Therefore, the buffer has to become saturated globally (i.e., in the entire presynaptic bouton) to cause significant FCT. The decay time course of facilitation will therefore be determined by the extrusion of  $\text{Ca}^{2+}$  by the plasmalemma transport proteins, with possible contribution of uptake into internal  $\text{Ca}^{2+}$  stores. Because we were interested in establishing an upper bound on maximal SF magnitude that can be achieved by the BSM, we made a conservative assumption about the  $\text{Ca}^{2+}$  extrusion rate in our simulations, choosing a clearance time estimate of 5 s, based on the crayfish NMJ measurements of Tank et al. (1995). This is much longer than the time scales of tens and hundreds of milliseconds that characterize the two compo-

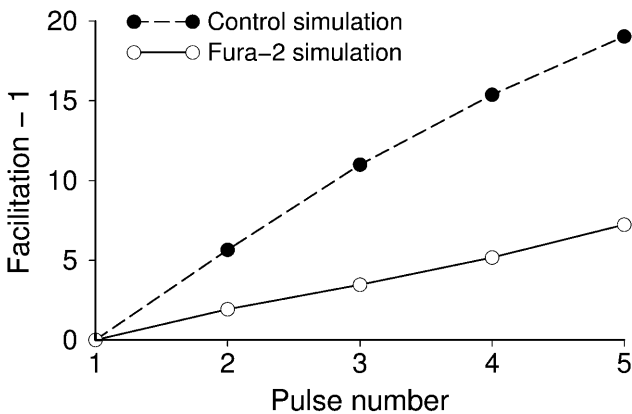


FIGURE 11 Facilitation grows sublinearly in the fixed buffer case. Shown is the simulated SF in response to a five-pulse 100-Hz AP train, arising from the saturation of a fixed buffer, with and without Fura-2. Note the sublinear accumulation time course, contrary to the mobile buffer case and the experimental data (cf. Fig. 7). Parameter values correspond to a point marked by + in Fig. 9 A ( $B_{\text{total}} = 11$  mM,  $K_D = 22$   $\mu\text{M}$ ,  $k_{\text{on}} = 0.2$   $\mu\text{M}^{-1}$   $\text{ms}^{-1}$ ;  $d = 60$  nm). Facilitation is normalized to zero for the first pulse. Fura-2 parameters are the same as in Fig. 7 A. The  $[\text{Ca}^{2+}]$  trace corresponding to the control simulation curve is shown in Fig. 9 Bb. The residual free  $\text{Ca}^{2+}$  contributes  $\sim 12\%$  to the fifth  $[\text{Ca}^{2+}]$  peak in the control simulation, and  $\sim 7\%$  in the Fura-2 simulation.

nents of SF decay observed at this synapse. The above estimate of  $\text{Ca}^{2+}$  clearance rate was obtained by tracking  $[\text{Ca}^{2+}]$  for tens of seconds after cessation of stimulation, when  $\text{Ca}^{2+}$  is low and the main mode of extrusion is through ATP-driven pumps. It is likely that immediately after stimulation the clearance proceeds at a faster rate, in particular due to activation of a lower-affinity but higher-capacity  $\text{Na}^+/\text{Ca}^{2+}$  exchanger, or some other low-affinity  $\text{Ca}^{2+}$  removal mechanism (e.g., a slow low-affinity buffer). Indeed, the decay of  $\text{Ca}^{2+}$  transients induced by AP trains was recently measured at the crayfish NMJ by Vyshedskiy and Lin (2000) on a finer time scale, revealing a biphasic decay with time constants of  $84 \pm 30$  and  $390 \pm 153$  ms. These time constants are comparable to the F1 ( $18 \pm 5$  ms) and F2 ( $530 \pm 200$  ms) components of facilitation decay at the crayfish NMJ (Zucker, 1974; Vyshedskiy and Lin, 1997; Tang et al., 2000). Note that due to the nonlinear dependence of transmitter release on  $\text{Ca}^{2+}$ , the SF decay times are expected to be somewhat shorter than the corresponding  $\text{Ca}^{2+}$  clearance time constants. Therefore, within the BSM framework, the decay time course of SF could be explained by the fast extrusion of  $\text{Ca}^{2+}$  from the terminal.

To allow for a faster decay of Ca transients, we have increased the pump dissociation constant from  $K_P = 0.2$   $\mu\text{M}$  to  $K_P = 5$   $\mu\text{M}$ , which is comparable to the affinity of the  $\text{Na}^+/\text{Ca}^{2+}$  exchanger (Blaustein and Lederer, 1999; Carafoli, 1987; DiPolo and Beauge, 1983), and increased the maximal extrusion rate from  $M = 0.01$   $\mu\text{M} \mu\text{m} \text{ms}^{-1}$  to  $M = 5$   $\mu\text{M} \mu\text{m} \text{ms}^{-1}$  (see Eq. 5). Fig. 12 A shows the resulting SF decay time course, with and without additional Fura-2. Note that our simulations predict a slowing of SF decay in the presence of an exogenous buffer such as Fura-2, contrary to experimental observations (cf. Fig. 12 C). The slower decay is explained by the fact that the  $\text{Ca}^{2+}$  clearance time is directly proportional to the total intraterminal buffering capacity (Neher and Augustine, 1992), which is approximately doubled after addition of 200  $\mu\text{M}$  of Fura-2. We verified that this effect is maintained if we assume that the

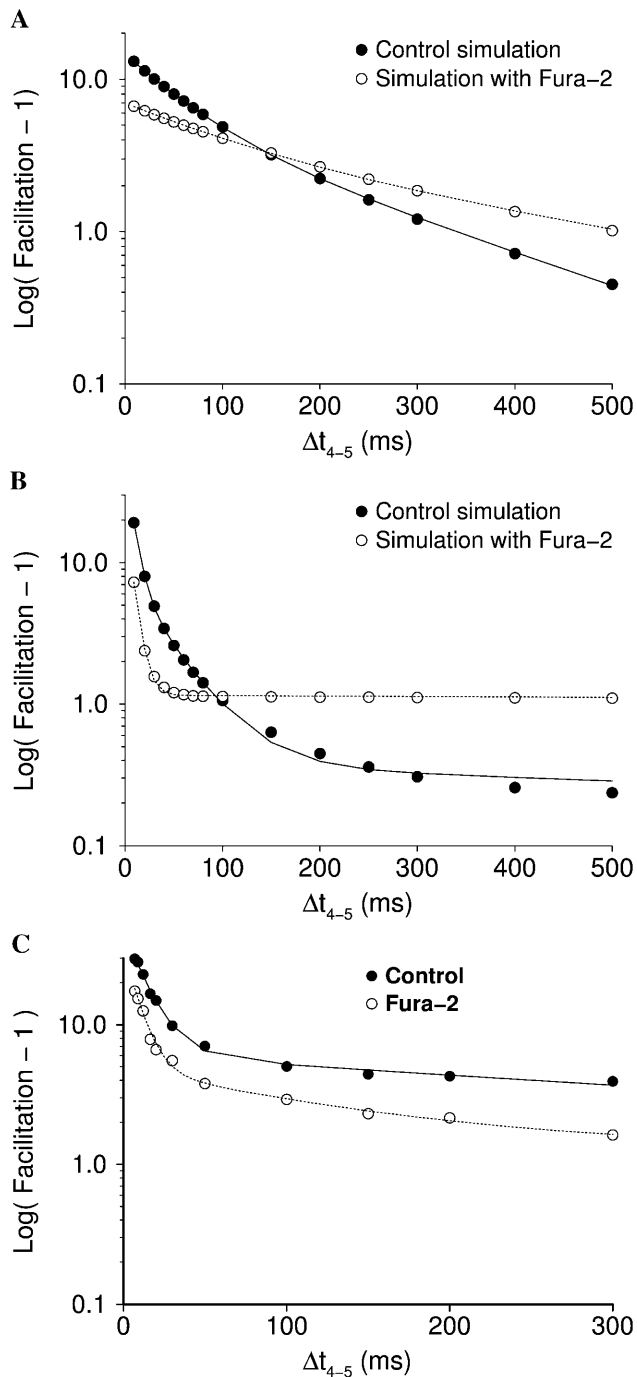


FIGURE 12 Experimental and simulated effect of Fura-2 application on the decay time course of SF. Shown is the SF magnitude for the last pulse in a 100-Hz five-pulse train, for a variable time interval between the fourth and the fifth pulses,  $\Delta t_{4-5}$ , for (A) mobile buffer simulation, (B) fixed buffer simulation, and (C) experimental data from Fig. 3 B of Tang et al. (2000). SF is computed as in Fig. 7. Parameter values in A are the same as in Fig. 7 A, except for the faster  $\text{Ca}^{2+}$  extrusion (see text), leading to a reduction of SF at  $\Delta t_{4-5} = 10$  ms from 19-fold to 14-fold. Parameter values in B are the same as in Fig. 11. The biexponential fits in A are given by  $9.4 \exp(-\Delta t/57 \text{ ms}) + 5.3 \exp(-\Delta t/202 \text{ ms})$  (●), and  $3.7 \exp(-\Delta t/111 \text{ ms}) + 3.3 \exp(-\Delta t/416 \text{ ms})$  (○). In B, fits are  $41 \exp(-\Delta t/7.9 \text{ ms}) + 7.1 \exp(-\Delta t/44 \text{ ms}) + 0.29 \exp(-\Delta t/6330 \text{ ms})$  (●), and  $21.7 \exp(-\Delta t/7.1 \text{ ms}) + 1.16$  (○).

Fura-2 is immobilized (Matveev et al., 2002), and in simulations where decay of  $\text{Ca}^{2+}$  transients is caused by a slow endogenous buffer (data not shown).

One may suggest therefore that the observed decay properties of SF are more consistent with a model relying on the saturation of a fixed buffer; as discussed above, it is a local rather than global saturation that causes FCT when buffers are fixed. Indeed, Figs. 10 and 9 B demonstrate that in the fixed buffer case the  $\text{Ca}^{2+}$  transients contain a gradually decaying ( $\tau \sim 10$  ms) component caused by the slow spatial reequilibration of  $\text{Ca}^{2+}$ , which is absent in the case of a mobile buffer (cf. Fig. 6 B). As we have shown previously (Matveev et al., 2002), this local free  $[\text{Ca}^{2+}]_{\text{res}}$  is responsible for SF in the two-site model of Tang et al. (2000). In the BSM framework, it partially contributes to SF by adding to the  $\text{Ca}^{2+}$  transients (Fig. 9 Bb; Eq. 10). Therefore, in the presence of fixed buffers the SF decay is expected to contain a fast (F1-like) phase due to the spatial reequilibration of  $\text{Ca}^{2+}$ , which should be strongly reduced in the presence of a mobile high-affinity  $\text{Ca}^{2+}$  buffer such as Fura-2, in agreement with experiment (Fig. 12 B). However, the second decay phase is slowed down in our simulations, as in the mobile buffer case (cf. Fig. 12 A). Thus, the model in its present form cannot successfully explain the experimentally observed effect of exogenous buffers on the decay time of SF, shown in Fig. 12 C (but see the Discussion below).

### FCT in the presence of two buffers

In this work we have concentrated on the case whereby a single dominant endogenous buffer is shaping the intracellular  $\text{Ca}^{2+}$  dynamics. We believe that a thorough investigation and understanding of the single-buffer situation is necessary before considering more complicated scenarios. However, one cannot exclude the possibility that several endogenous buffers make a commensurate contribution to the overall buffering capacity at the crayfish NMJ, as well as at other synapses. In particular, one may propose that the immobile or poorly mobile buffer with low capacity ( $\kappa_0 \sim 40\text{--}50$ ) found in different cell types (references cited in Results) represents the basal buffer present in all synapses, whereas only a subset of cell types possess an additional mobile high-capacity buffer (e.g., calbindin; Nägerl et al., 2000). Although the data on the properties of the putative immobile low-capacity buffer is lacking, evidence from chromaffin cell studies suggest that it may have low affinity (Xu et al., 1997). Therefore, to analyze this possibility we performed simulations in which a mobile buffer with varying  $B_{\text{total}}$  and  $k_{\text{on}}$  was added to a fixed concentration of a low-affinity immobile buffer with  $B_{\text{total}} = 750 \mu\text{M}$ ,  $K_D = 15 \mu\text{M}$  ( $\kappa_0 = 50$ ), and  $k_{\text{on}} = 0.1 \mu\text{M}^{-1} \text{ms}^{-1}$  (Fig. 13). Our results show that the FCT is reduced when the low-affinity buffer is introduced, and that the size of this reduction depends on the relative capacities of the

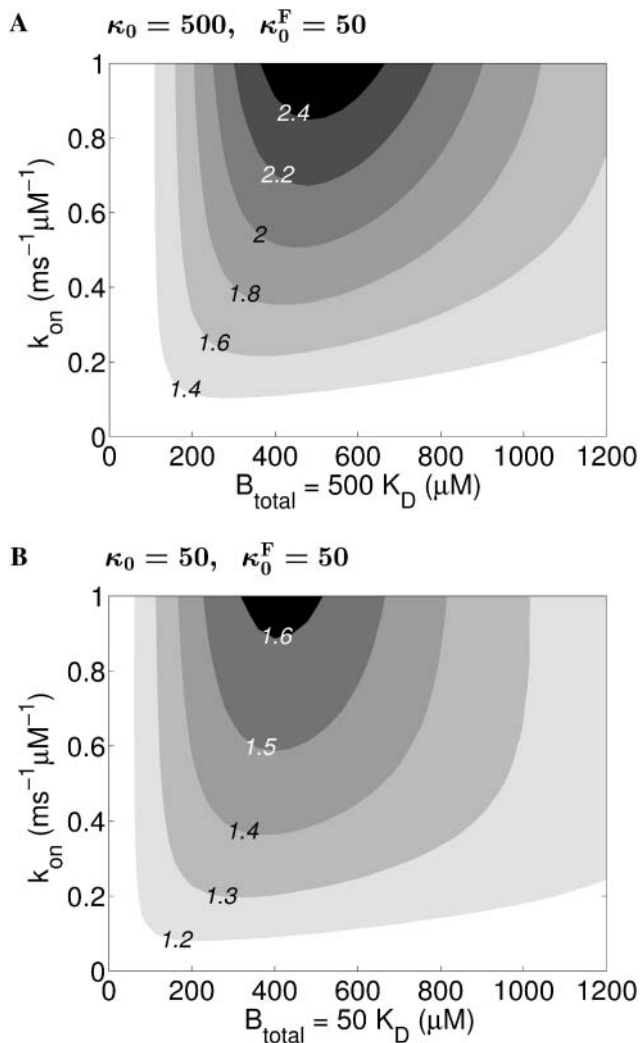


FIGURE 13 Dependence of FCT on the properties of a mobile buffer, in the presence of an immobile low-affinity buffer with fixed characteristics. Five-pulse FCT is shown as a function of  $k_{\text{on}}$  and  $B_{\text{total}}$  of the mobile buffer, for mobile buffering capacity of (A)  $\kappa_0 = 500$  and (B)  $\kappa_0 = 50$ . The buffering capacity of the immobile low-affinity buffer is  $\kappa_0^F = 50$ , in both panels. The properties of the immobile buffer are fixed:  $B_{\text{total}} = 750 \mu\text{M}$ ,  $K_D = 15 \mu\text{M}$ , and  $k_{\text{on}} = 0.1 \mu\text{M}^{-1} \text{ms}^{-1}$ . Other parameters are the same as in Figs. 2–4 ( $D_B = 0.2 \mu\text{m}^2 \text{ms}^{-1}$ ,  $I_{\text{Ca}} = 11.7 \text{ pA}$ ,  $d = 60 \text{ nm}$ ). Note that introducing an immobile low-affinity buffer reduces FCT, as compared to the single-buffer case (Fig. 5). The magnitude of this reduction is more dramatic when the capacities of the two buffers are comparable (cf. panel B and Fig. 5 B).

two buffers. Namely, the maximal achievable FCT is more significantly reduced when the immobile and mobile buffers have equal capacities (Fig. 13 B), whereas the FCT reduction is less dramatic when the capacity of the mobile buffer is significantly higher than the capacity of the low-affinity fixed buffer (Fig. 13 A). In general, we could not find conditions under which a two-buffer system would yield a higher FCT magnitude as compared to a single buffer system (data not shown). This puts an additional emphasis on the point that the FCT magnitude that we

demonstrate is the maximal bound on the FCT that can be achieved under physiological conditions.

## DISCUSSION

Using a computer model of a crayfish motor bouton, we have explored in detail the phenomenon of facilitation of  $\text{Ca}^{2+}$  transients resulting from the saturation of an endogenous  $\text{Ca}^{2+}$  buffer. We have given an exhaustive characterization of the dependence of FCT on the endogenous buffering parameters (Table 2), and have described the conditions necessary to obtain a sufficiently high SF magnitude, as summarized below. The requirement of significant distance between the  $\text{Ca}^{2+}$  source and the secretion site; our findings on the nonmonotonic dependence of FCT on buffer concentration; and the increase of FCT with increasing  $[\text{Ca}^{2+}]_{\text{ext}}$ , are all consistent with the experimental results of Blatow et al. (2003).

Further, we compare our simulation results with the properties of SF observed at the crayfish NMJ by Tang et al. (2000). The crayfish NMJ is particularly well suited for the study of SF, because it displays pronounced SF under physiological conditions, and the increase of synaptic response is not occluded by concomitant synaptic depression, which is the case in most other systems (reviewed by Zucker and Regehr, 2002).

### FCT and buffer mobility

As we have shown, buffer mobility is a crucial factor in the BSM. Curiously, we found that to achieve a physiologically relevant SF magnitude, the buffer has to be either highly mobile or highly immobilized, with much smaller FCT achieved for intermediate values of mobility (Fig. 8 B). This is because the mechanism by which buffer saturation causes facilitation is different in the high- versus low-mobility regimes. A highly mobile buffer efficiently carries  $\text{Ca}^{2+}$  ions away from the AZ, strongly shunting the response to the first pulses in a stimulation train, while becoming gradually saturated in the entire bouton (Fig. 2). This results in large FCT. A fixed buffer causes facilitation by saturating locally, rather than globally, which traps  $\text{Ca}^{2+}$  ions in an area surrounding the AZ (Fig. 10; Nowycky and Pinter, 1993; Neher, 1998a). To absorb a significant fraction of the  $\text{Ca}^{2+}$  influx locally, the buffer has to be completely immobile, and its concentration has to be much higher than in the mobile buffer case, extending into the range of unrealistically high values (Figs. 8 B and 9). Further, achieving high saturation also requires a significant separation between the  $\text{Ca}^{2+}$  sensor and the  $\text{Ca}^{2+}$  source. However, at larger distances and higher  $B_{\text{total}}$ , the free  $[\text{Ca}^{2+}]_{\text{res}}$  becomes comparable in magnitude to the fast  $\text{Ca}^{2+}$  transients, providing a greater contribution to the overall facilitation (Eq. 10). At large enough values of distance and  $B_{\text{total}}$ , the peak in  $\text{Ca}^{2+}$  concentration becomes significantly delayed with respect to

the end of the  $\text{Ca}^{2+}$  influx (Fig. 9 *Bc*), because diffusion is slowed by the fixed buffer, and the trapped  $\text{Ca}^{2+}$  ions undergo multiple binding/unbinding steps before they reach their secretory target. Under these conditions, a single release site model is no longer consistent with the transient nature of the postsynaptic response. Therefore, the model would have to be expanded to include a proximal secretory trigger, in addition to the more distal facilitation site, as proposed by Tang et al. (2000) and explored more recently by Matveev et al. (2002). The proximal site would preserve the transient nature of transmitter release, because sufficiently close to the channel cluster the decay of  $\text{Ca}^{2+}$  peaks is fast.

In the present simulations, in the fixed buffer case the mechanism of facilitation undergoes a gradual qualitative change as the parameters are varied, and at high values of distance and  $B_{\text{total}}$ , the accumulation of free  $[\text{Ca}^{2+}]_{\text{res}}$  becomes the principle source of facilitation (Fig. 9 *Bc*). For intermediate values of parameters, buffer saturation begins to contribute to the overall facilitation magnitude (Fig. 9 *Bb*). In contrast, in the mobile buffer case the FCT through buffer saturation represents the only mechanism of SF for a wide range of buffering conditions. These results further illustrate the opposing effects of fixed and mobile buffers on  $\text{Ca}^{2+}$  dynamics, elucidated in earlier studies (Junge and McLaughlin, 1987; Sala and Hernández-Cruz, 1990; Zhou and Neher, 1993; Nowycky and Pinter, 1993; Winslow et al., 1994; Gabso et al., 1997; Naraghi and Neher, 1997; Neher, 1998a).

### Nonmonotonic dependence on buffer concentration

Most studies show a reduction in SF upon introduction of exogenous mobile  $\text{Ca}^{2+}$  buffers, pointing to the importance of residual  $\text{Ca}^{2+}$  as the main source of SF (reviewed in Zucker and Regehr, 2002). Our results suggest that this effect is consistent with the BSM (Figs. 7, 11, and 12). However, depending on whether the endogenous buffering conditions correspond to the “ascending” or the “descending” slope of the FCT peak in Fig. 3, and depending on the mobility of the added buffer relative to the endogenous one, one would predict either an increase or a decrease in the facilitation magnitude. Further, regardless of the source of SF under physiological conditions, adding an alien mobile  $\text{Ca}^{2+}$  buffer may change the physiological mechanism of facilitation to that of FCT. Such “pseudofacilitation” (Neher, 1998a) may turn out to be greater in magnitude than the native facilitation under control conditions, but as Fig. 3 suggests, it would inevitably decline as the concentration of the added buffer is ramped up sufficiently. This agrees completely with the “pseudofacilitation” effect that has been observed at some neocortical and hippocampal synapses in response to BAPTA application (see Fig. 9 *B* in Rozov et al., 2001, and Fig. 3 *B* of Blatow et al., 2003). Pseudofacilitation may also explain the discrepancy between the results of Winslow et al. (1994), showing the lack of effect of BAPTA-

acetoxymethyl-ester on facilitation at the crayfish NMJ, and the results of other studies showing that similar manipulations reduce facilitation in this system. It may be argued that the particular concentration of BAPTA-acetoxymethyl-ester used by Winslow et al. caused a pseudofacilitation effect that balanced the concomitant reduction of facilitation occurring through a different mechanism (see also Discussion in Bennett et al., 2000).

### Dependence on external $\text{Ca}^{2+}$ concentration

The dependence of FCT on the buffer concentration (and hence, on its affinity  $K_D$ , as well) remains nonmonotonic, even if the value of  $\kappa_0$  is kept fixed (Figs. 5, 6 *A*, and 9 *A*). It follows then that the dependence of FCT on  $I_{\text{Ca}}$  is also nonmonotonic, because changing the value of  $I_{\text{Ca}}$  is equivalent to a simultaneous rescaling of the parameters  $B_{\text{total}}$  and  $K_D$  in the opposite direction (Figs. 3 *A* and 5 *A*). A consequence of this fact is that the FCT is an increasing function of the external  $\text{Ca}^{2+}$ ,  $[\text{Ca}^{2+}]_{\text{ext}}$ , for small enough values of  $[\text{Ca}^{2+}]_{\text{ext}}$  assuming that  $I_{\text{Ca}}$  is proportional to  $[\text{Ca}^{2+}]_{\text{ext}}$ . This agrees with the experimental results of Blatow et al. (2003) and Rozov et al. (2001). However, at sufficiently high values of  $[\text{Ca}^{2+}]_{\text{ext}}$ , the dependence of SF on  $[\text{Ca}^{2+}]_{\text{ext}}$  should reverse. Further, the saturation of the putative secretory site and the potential emergence of short-term synaptic depression at higher release rates, two effects not included in our model, would limit the range of  $[\text{Ca}^{2+}]_{\text{ext}}$  values for which SF grows with  $[\text{Ca}^{2+}]_{\text{ext}}$ .

### Dependence on the properties of the release mechanism

As discussed above, we have chosen to quantify facilitation solely in terms of the increase in the  $\text{Ca}^{2+}$  concentration. Inclusion of a specific  $\text{Ca}^{2+}$ -dependent vesicle release scheme would obscure the relationship between the facilitation magnitude and the  $\text{Ca}^{2+}$ -binding properties of the buffer. Saturation of the release mechanism at high  $[\text{Ca}^{2+}]$  would reduce SF estimates calculated according to Eqs. 9 and 10, especially at low values of  $B_{\text{total}}$  and  $k_{\text{on}}$ , and for small separations between the  $\text{Ca}^{2+}$  channel and the release site, because these conditions correspond to high  $\text{Ca}^{2+}$  concentration. Therefore, saturation effects would move the FCT peak in parameter sweep plots of Figs. 3, 5, 6, 8, and 9 to higher values of  $B_{\text{total}}$ , and the height of the peak may be significantly reduced. However, all our conclusions about the qualitative dependence of FCT on the endogenous buffering parameters would remain unchanged.

### Facilitation accumulation time course

We have found that the saturation of either a very mobile or a completely immobilized buffer may explain the magnitude

of SF observed at the crayfish NMJ (Figs. 7 and 11). However, the observed supralinear accumulation time course of SF is only predicted if the endogenous buffer is mobile. In agreement with our results, experiments of Blatow et al. (2003) reveal a supralinear SF growth at a hippocampal mossy fiber synapse that contains a highly mobile calbindin (see Fig. 5 C therein; properties of calbindin have been described by Nägerl et al., 2000). Note also that lowering the assumed  $\text{Ca}^{2+}$ -cooperativity of release from four to three, and including saturation at high  $\text{Ca}^{2+}$  levels, would make the simulated SF growth less steep, favoring even more the mobile buffer model over the fixed buffer case.

It is important to bear in mind that our results show the upper bound on the physiologically attainable level of SF. Therefore, even in the more favorable mobile buffer case, the parameter region corresponding to the observed magnitude of SF may be more narrow than our results in Figs. 3, 5, 6, and 13 suggest, in particular because we assume very high buffer mobility and a nonsaturating relationship between transmitter release and  $[\text{Ca}^{2+}]$ .

### Acceleration of facilitation decay by exogenous buffers

Although saturation of a mobile buffer can successfully explain the observed magnitude and accumulation time course of SF, we showed that it is not consistent with the observed acceleration of decay of SF by fast high-affinity exogenous buffers (Fig. 12, A and C). In the fixed buffer case, the faster phase of decay, corresponding to the spatial reequilibration of the locally elevated residual  $\text{Ca}^{2+}$ , would be indeed accelerated upon adding a mobile buffer. Still, the slower decay phase, corresponding to  $\text{Ca}^{2+}$  clearance, would be slowed down, as in the mobile buffer case (Fig. 12 B). However, one may suggest that a slow leak of  $\text{Ca}^{2+}$  from the bouton into the axonal compartment, an effect not included in our model, may make a significant contribution to the decay of SF. If the mobility of the exogenous buffer is greater than or equal to the mobility of the endogenous one, then its addition would accelerate the putative leak of  $\text{Ca}^{2+}$  into the axon, thereby accelerating SF decay. It is not clear, however, whether the faster decay of both components of SF could be explained by this leak mechanism. Further, recent crayfish NMJ experiments by J.-Y. Lin, Q. Fu, and T. Allana (in preparation) show that the decay of  $\text{Ca}^{2+}$  transients on timescales of tens to hundreds of milliseconds is not sensitive to the mobility of the  $\text{Ca}^{2+}$ -sensitive dye used to image  $[\text{Ca}^{2+}]$ , arguing against the importance of this leak. The above study also suggests that the endogenous Ca buffers at the crayfish opener NMJ are characterized by low mobility. Therefore, it is unlikely that BSM can explain the observed properties of SF at the crayfish NMJ. However, further modeling work that would incorporate this new experimental data is necessary to reach a definite conclusion. Parenthet-

ically, we note that at the frog NMJ, addition of exogenous buffer does slow the decay of SF (Robitaille and Charlton, 1991), as predicted by the present model.

We showed previously (Matveev et al., 2002) that both the growth and the decay properties of SF at the crayfish NMJ can be explained by a model with a distant facilitation site proposed by Tang et al. (2000). However, to explain the supralinear accumulation time course, the two-site model had to incorporate additional assumptions of a very large separation between the SF sensor and the  $\text{Ca}^{2+}$  channel array ( $>250$  nm), or a high degree of tortuosity near the active zone. The two-site model is similar to the BSM in that both rely exclusively on the dynamics of  $\text{Ca}^{2+}$  diffusion and buffering to explain the observed behavior of SF, in particular its decay time course. An alternative possibility is that at least one of the facilitation decay components may result from the slow unbinding of  $\text{Ca}^{2+}$  from a release-controlling  $\text{Ca}^{2+}$  sensor (Yamada and Zucker, 1992; Bertram et al., 1996; Bennett et al., 1997; Dittman et al., 2000). In its pure form, such a bound  $\text{Ca}^{2+}$  model is inconsistent with experimental data demonstrating the importance of free residual  $\text{Ca}^{2+}$  for SF (reviewed in Zucker and Regehr, 2002). Yet it is possible that a hybrid model, sensitive to free  $\text{Ca}^{2+}$  but including a slow unbinding process, could also reproduce the facilitation behavior observed at the crayfish NMJ. Although recent experiments have ruled out the existence of a slow unbinding step at the calyx of Held terminal (Felmy et al., 2003), it was shown to play a role at a cerebellar granule cell synapse (Atluri and Regehr, 1996).

Our analysis shows that the buffer saturation mechanism (better termed the FCT model) and the two-site residual free  $\text{Ca}^{2+}$  model can be viewed as being on the opposite sides of the same spectrum (Fig. 8 B). Whereas the FCT is most pronounced when a highly mobile buffer saturates globally, the accumulation of free  $[\text{Ca}^{2+}]_{\text{res}}$  is mediated by the local saturation of (local  $\text{Ca}^{2+}$  trapping by) a high-concentration fixed buffer. However, there exists an intermediate parameter regime, where the accumulation of free  $[\text{Ca}^{2+}]_{\text{res}}$  and the facilitation of  $\text{Ca}^{2+}$  transients can both contribute to synaptic facilitation (Fig. 9 Bb).

### APPENDIX: THE CASE OF NONZERO RESTING $\text{Ca}^{2+}$ CONCENTRATION

Although our simulations assume zero resting  $\text{Ca}^{2+}$  concentration,  $\text{Ca}_{\text{rest}}$ , the results can be straightforwardly translated to the case of nonzero  $\text{Ca}_{\text{rest}}$ . The  $\text{Ca}_{\text{rest}}$  is a constant term not affecting the dynamics of diffusion or buffering, so its effect is limited to a transformation of model parameters. Let's express the total  $[\text{Ca}^{2+}]$  as a sum of  $\text{Ca}_{\text{rest}}$  and the contribution due to  $\text{Ca}^{2+}$  entry during an action potential ( $[\text{Ca}^{2+}] \equiv [\text{Ca}^{2+}]_{\text{AP}}$ ):  $[\text{Ca}^{2+}]_{\text{total}} = \text{Ca}_{\text{rest}} + [\text{Ca}^{2+}]$ . Because the derivative of the constant resting term  $\text{Ca}_{\text{rest}}$  on the left- and the right-hand sides of Eq. 2 is zero, the only change is in the reaction term on the right-hand side of Eqs. 2 and 3:

$$R = -k_{\text{on}}[B][\text{Ca}^{2+}] + k_{\text{off}}(B_{\text{total}} - [B]). \quad (11)$$



Let us now introduce the resting concentration of free buffer,  $B_{\text{rest}}$ , in equilibrium with the resting  $\text{Ca}^{2+}$ :

$$k_{\text{on}} C a_{\text{rest}} B_{\text{rest}} = k_{\text{off}} (B_{\text{total}} - B_{\text{rest}}). \quad (12)$$

$$B_{\text{rest}} = \frac{B_{\text{total}} K_{\text{D}}}{C a_{\text{rest}} + K_{\text{D}}}, \quad \text{where } K_{\text{D}} = \frac{k_{\text{off}}}{k_{\text{on}}}. \quad (13)$$

We can then express the reaction term as

$$R = -k_{\text{on}} [B] (C a_{\text{rest}} + [C a^{2+}]) + k_{\text{off}} (B_{\text{total}} - B_{\text{rest}}) + k_{\text{off}} (B_{\text{rest}} - [B]). \quad (14)$$

Using Eq. 12 to eliminate the second term in above expression, this yields

$$R = -k_{\text{on}} [B] (C a_{\text{rest}} + [C a^{2+}]) + k_{\text{on}} C a_{\text{rest}} B_{\text{rest}} + k_{\text{off}} (B_{\text{rest}} - [B]) \\ = -k_{\text{on}} [B] [C a^{2+}] + (k_{\text{off}} + k_{\text{on}} C a_{\text{rest}}) (B_{\text{rest}} - [B]). \quad (15)$$

Now, notice that the reaction term has the same form as in the  $C a_{\text{rest}} = 0$  case (Eq. 11), except that  $B_{\text{total}}$  has to be replaced with  $B_{\text{rest}}$  (given by Eq. 13), and  $k_{\text{off}}$  has to be replaced with  $k_{\text{off}} + k_{\text{on}} C a_{\text{rest}}$ , which in turn implies that  $K_{\text{D}}$  has to be replaced with  $K_{\text{D}} + C a_{\text{rest}}$ . Note that this parameter transformation allows us to recover the expression for the rest-state buffering ratio  $\kappa_0$  in the nonzero  $C a_{\text{rest}}$  case (Eq. 6):

$$\kappa_0 = \frac{B'_{\text{total}}}{K'_{\text{D}}} = \frac{B_{\text{rest}}}{K_{\text{D}} + C a_{\text{rest}}} = \frac{B_{\text{total}} K_{\text{D}}}{(K_{\text{D}} + C a_{\text{rest}})^2}, \quad (16)$$

where the primed parameters correspond to the case of zero  $C a_{\text{rest}}$ . As expected, the value of the buffering ratio is invariant with respect to this parameter change.

Thus, to recover the dependence of facilitation on model parameters for the case of nonzero  $C a_{\text{rest}}$ , the inverse of the above transformations has to be applied to the parameter values in Figs. 2–13:

$$B_{\text{total}} = \frac{B'_{\text{total}}}{1 - C a_{\text{rest}}/K'_{\text{D}}}, \\ k_{\text{off}} = k'_{\text{off}} \left( 1 - \frac{C a_{\text{rest}}}{K'_{\text{D}}} \right), \\ K_{\text{D}} = K'_{\text{D}} - C a_{\text{rest}}, \quad (17)$$

where  $K'_{\text{D}} > C a_{\text{rest}}$ . Note that the value of  $k_{\text{on}}$  remains unaltered by this substitution. The condition  $K'_{\text{D}} > C a_{\text{rest}}$  implies that the magnitude of  $C a_{\text{rest}}$  imposes a constraint on the relevant range of values of  $K'_{\text{D}}$ . Given a certain value of  $C a_{\text{rest}}$ , one should ignore those parts of Figs. 3, 5, 6, and 13 that lie in the region  $K'_{\text{D}} < C a_{\text{rest}}$ . The transformations described by Eq. 17 will have no effect on the results for the fixed buffer case (Fig. 9), because the value of  $K'_{\text{D}}$  is much greater than  $C a_{\text{rest}}$  in the relevant parameter range. In the mobile buffer case, for the fixed- $\kappa_0$  plots showing the dependence of facilitation on  $B'_{\text{total}}$  ( $K'_{\text{D}}$ ) and  $k_{\text{on}}$  (Figs. 5 and 6), these transformations involve a simple shift to the left by the amount equal to  $C a_{\text{rest}}$ , after the abscissa values are reinterpreted in terms of  $K'_{\text{D}}$  instead of  $B'_{\text{total}}$ . Note that the constant- $\kappa_0$  proportionality relationship between  $K_{\text{D}}$  and  $B_{\text{total}}$  no longer holds in this case, but is determined according to Eq. 6:

$$B_{\text{total}} = \kappa_0 K_{\text{D}} (1 + C a_{\text{rest}}/K_{\text{D}})^2. \quad (18)$$

Assuming for example  $C a_{\text{rest}} = 0.1 \mu\text{M}$ , the facilitation peak in Figs. 5 A and 6 Ab at  $\{k_{\text{on}} = 1 \mu\text{M}^{-1} \text{ms}^{-1}, B'_{\text{total}} = 400 \mu\text{M}, K'_{\text{D}} = 0.8 \mu\text{M}\}$  corresponds to  $\{B_{\text{total}} = 457 \mu\text{M}, K_{\text{D}} = 0.7 \mu\text{M}\}$ . In Fig. 3, where the values of  $B'_{\text{total}}$  and  $K'_{\text{D}}$  ( $k'_{\text{on}}$ ) are independently varied, the transformation to the nonzero  $C a_{\text{rest}}$  would involve a downward shift along the  $K'_{\text{D}}$  axis by  $C a_{\text{rest}}$ , as well as a nonhomogenous stretch to the right, shifting the facilitation peak to higher

values of  $B'_{\text{total}}$ . The latter shift in the  $B_{\text{total}}$  direction is more significant for lower values of  $K'_{\text{D}}$ . Further, the value of  $k_{\text{off}}$  will not remain constant throughout panels A and B, due to its dependence on  $K'_{\text{D}}$  (see Eq. 17). Thus, the independence of facilitation on the value of  $k_{\text{off}}$  in the mobile buffer case (Fig. 3) is only approximate, holding for values of  $K_{\text{D}} \gg C a_{\text{rest}}$ .

## REFERENCES

- Allbritton, N. L., T. Meyer, and L. Stryer. 1992. Range of messenger action of calcium ion and inositol 1,4,5-trisphosphate. *Science*. 258:1812–1815.
- Atluri, P. P., and W. G. Regehr. 1996. Determinants of the time course of facilitation at the granule cell to Purkinje cell synapse. *J. Neurosci.* 16:5661–5671.
- Atwood, H. L., and S. Karunanithi. 2002. Diversification of synaptic strength: presynaptic elements. *Nat. Rev. Neurosci.* 3:497–516.
- Atwood, H. L., S. Karunanithi, J. Georgiou, and M. P. Charlton. 1997. Strength of synaptic transmission at neuromuscular junctions of crustaceans and insects in relation to calcium entry. *Invert. Neurosci.* 3:81–87.
- Bennett, M. R., W. G. Gibson, and J. Robinson. 1997. Probabilistic secretion of quanta and the synaptosome hypothesis: evoked release at active zones of varicosities, boutons, and endplates. *Biophys. J.* 73:1815–1829.
- Bennett, M. R., L. Farnell, and W. G. Gibson. 2000. The probability of quantal secretion within an array of calcium channels of an active zone. *Biophys. J.* 78:2222–2240.
- Bertram, R., A. Sherman, and E. Stanley. 1996. The single domain/bound calcium hypothesis of transmitter release and facilitation. *J. Neurophysiol.* 75:1919–1931.
- Blatow, M., A. Caputi, N. Burnashev, H. Monyer, and A. Rozov. 2003.  $\text{Ca}^{2+}$  buffer saturation underlies paired pulse facilitation in calbindin-D28k-containing terminals. *Neuron*. 38:79–88.
- Blaustein, M. P., and W. J. Lederer. 1999. Sodium/calcium exchange: its physiological implications. *Physiol. Rev.* 79:763–854.
- Bollmann, J. H., B. Sakmann, and J. G. Borst. 2000. Calcium sensitivity of glutamate release in a calyx-type terminal. *Science*. 289:953–957.
- Burrone, J., G. Neves, A. Gomis, A. Cooke, and L. Lagnado. 2002. Endogenous calcium buffers regulate fast exocytosis in the synaptic terminal of retinal bipolar cells. *Neuron*. 33:101–112.
- Carafoli, E. 1987. Intracellular calcium homeostasis. *Annu. Rev. Biochem.* 56:395–433.
- Catterall, W. A. 1999. Interactions of presynaptic  $\text{Ca}^{2+}$  channels and snare proteins in neurotransmitter release. *Ann. N. Y. Acad. Sci.* 868:144–159.
- Chad, J. E., and R. Eckert. 1984. Calcium domains associated with individual channels can account for anomalous voltage relations of Ca-dependent responses. *Biophys. J.* 45:993–999.
- Cooper, R. L., L. Marin, and H. L. Atwood. 1995. Synaptic differentiation of a single motor neuron: conjoint definition of transmitter release, presynaptic calcium signals, and ultrastructure. *J. Neurosci.* 15:4209–4222.
- Cooper, R. L., J. L. Winslow, C. K. Govind, and H. L. Atwood. 1996. Synaptic structural complexity as a factor enhancing probability of calcium-mediated transmitter release. *J. Neurophysiol.* 75:2451–2466.
- Delaney, K. R., and D. W. Tank. 1994. A quantitative measurement of the dependence of short-term synaptic enhancement on presynaptic residual calcium. *J. Neurosci.* 14:5885–5902.
- Dipolo, R., and L. Beauge. 1983. The calcium pump and sodium-calcium exchange in squid axons. *Annu. Rev. Physiol.* 45:313–324.
- Dittman, J. S., A. C. Kreitzer, and W. G. Regehr. 2000. Interplay between facilitation, depression, and residual calcium at three presynaptic terminals. *J. Neurosci.* 20:1374–1385.
- Felmy, F. E., E. Neher, and R. Schneggenburger. 2003. Probing the intracellular calcium sensitivity of transmitter release during synaptic facilitation. *Neuron*. 37:801–811.

- Fisher, S. A., T. M. Fischer, and T. J. Carew. 1997. Multiple overlapping processes underlying short-term synaptic enhancement. *Trends Neurosci.* 20:170–177.
- Fisher, T. E., and C. W. Bourque. 2001. The function of  $\text{Ca}^{2+}$  channel subtypes in exocytotic secretion: new perspectives from synaptic and non-synaptic release. *Prog. Biophys. Mol. Biol.* 77:269–303.
- Fogelson, A. L., and R. S. Zucker. 1985. Presynaptic calcium diffusion from various arrays of single channels. Implications for transmitter release and synaptic facilitation. *Biophys. J.* 48:1003–1017.
- Gabso, M., E. Neher, and M. E. Spira. 1997. Low mobility of the  $\text{Ca}^{2+}$  buffers in axons of cultured Aplysia neurons. *Neuron.* 18:473–481.
- Helmchen, F., J. G. Borst, and B. Sakmann. 1997. Calcium dynamics associated with a single action potential in a CNS presynaptic terminal. *Biophys. J.* 72:1458–1471.
- Helmchen, F., K. Imoto, and B. Sakmann. 1996.  $\text{Ca}^{2+}$  buffering and action potential-evoked  $\text{Ca}^{2+}$  signaling in dendrites of pyramidal neurons. *Biophys. J.* 70:1069–1081.
- Hines, M. 1984. Efficient computation of branched nerve equations. *Int. J. Biomed. Comput.* 15:69–76.
- Irving, M., J. Maylie, N. L. Sizto, and W. K. Chandler. 1990. Intracellular diffusion in the presence of mobile buffers. Application to proton movement in muscle. *Biophys. J.* 57:717–721.
- Jackson, M. B., and S. J. Redman. 2003. Calcium dynamics, buffering, and buffer saturation in the boutons of dentate granule-cell axons in the hilus. *J. Neurosci.* 23:1612–1621.
- Jarvis, S. E., and G. W. Zamponi. 2001. Interactions between presynaptic  $\text{Ca}^{2+}$  channels, cytoplasmic messengers and proteins of the synaptic vesicle release complex. *Trends Pharmacol. Sci.* 22:519–525.
- Junge, W., and S. McLaughlin. 1987. The role of fixed and mobile buffers in the kinetics of proton movement. *Biochim. Biophys. Acta.* 890: 1–5.
- Katz, B., and R. Miledi. 1968. The role of calcium in neuromuscular facilitation. *J. Physiol.* 195:481–492.
- Keizer, J. 1987. Diffusion effects on rapid bimolecular chemical reactions. *Chem. Rev.* 87:167–180.
- Klingauf, J., and E. Neher. 1997. Modeling buffered  $\text{Ca}^{2+}$  diffusion near the membrane: implications for secretion in neuroendocrine cells. *Biophys. J.* 72:674–690.
- Landò, L., and R. S. Zucker. 1994.  $\text{Ca}^{2+}$  cooperativity in neurosecretion measured using photolabile  $\text{Ca}^{2+}$  chelators. *J. Neurophysiol.* 72:825–830.
- Lee, S. H., C. Rosenmund, B. Schwaller, and E. Neher. 2000. Differences in  $\text{Ca}^{2+}$  buffering properties between excitatory and inhibitory hippocampal neurons from the rat. *J. Physiol.* 525:405–418.
- Maeda, H., G. C. Ellis-Davies, K. Ito, Y. Miyashita, and H. Kasai. 1999. Supralinear  $\text{Ca}^{2+}$  signaling by cooperative and mobile  $\text{Ca}^{2+}$  buffering in Purkinje neurons. *Neuron.* 24:989–1002.
- Magleby, K. L. 1987. Short-term changes in synaptic efficacy. In *Synaptic Function*. G. Edelman, W. Gall, and W. Cowan, editors. Wiley, New York. 21–56.
- Matveev, V., A. Sherman, and R. S. Zucker. 2002. New and corrected simulations of synaptic facilitation. *Biophys. J.* 83:1368–1373.
- Meinrenken, C. J., J. G. Borst, and B. Sakmann. 2002. Calcium secretion coupling at calyx of Held governed by nonuniform channel-vesicle topography. *J. Neurosci.* 22:1648–1667.
- Morton, K. W., and D. F. Mayers. 1994. *Numerical Solution of Partial Differential Equations: An Introduction*. University Press, Cambridge, UK.
- Nägerl, U. V., D. Novo, I. Mody, and J. L. Vergara. 2000. Binding kinetics of calbindin-D(28k) determined by flash photolysis of caged  $\text{Ca}^{2+}$ . *Biophys. J.* 79:3009–3018.
- Naraghi, M., and E. Neher. 1997. Linearized buffered  $\text{Ca}^{2+}$  diffusion in microdomains and its implications for calculation of  $[\text{Ca}^{2+}]$  at the mouth of a calcium channel. *J. Neurosci.* 17:6961–6973.
- Neher, E. 1998a. Usefulness and limitations of linear approximations to the understanding of  $\text{Ca}^{2+}$  signals. *Cell Calcium.* 24:345–357.
- Neher, E. 1998b. Vesicle pools and  $\text{Ca}^{2+}$  microdomains: new tools for understanding their roles in neurotransmitter release. *Neuron.* 20:389–399.
- Neher, E., and G. J. Augustine. 1992. Calcium gradients and buffers in bovine chromaffin cells. *J. Physiol.* 450:273–301.
- Nowycky, M. C., and M. J. Pinter. 1993. Time courses of calcium and calcium-bound buffers following calcium influx in a model cell. *Biophys. J.* 64:77–91.
- Ohana, O., and B. Sakmann. 1998. Transmitter release modulation in nerve terminals of rat neocortical pyramidal cells by intracellular calcium buffers. *J. Physiol.* 513:135–148.
- Ohnuma, K., M. D. Whim, R. D. Fetter, L. K. Kaczmarek, and R. S. Zucker. 2001. Presynaptic target of  $\text{Ca}^{2+}$  action on neuropeptide and acetylcholine release in *Aplysia californica*. *J. Physiol.* 535:647–662.
- Pape, P. C., D.-S. Jong, and W. K. Chandler. 1998. Effects of partial sarcoplasmic reticulum calcium depletion on calcium release in frog cut muscle fibers equilibrated with 20 mM EGTA. *J. Gen. Physiol.* 112: 263–295.
- Rahamimoff, R. 1968. A dual effect of calcium ions on neuromuscular facilitation. *J. Physiol.* 195:471–480.
- Ravin, R., H. Parnas, M. E. Spira, N. Volfovsky, and I. Parnas. 1999. Simultaneous measurement of evoked release and  $[\text{Ca}^{2+}]_i$  in a crayfish release bouton reveals high affinity of release to  $\text{Ca}^{2+}$ . *J. Neurophysiol.* 81:634–642.
- Regehr, W. G., K. R. Delaney, and D. W. Tank. 1994. The role presynaptic calcium in short-term enhancement at the hippocampal mossy fiber synapse. *J. Neurosci.* 14:523–537.
- Roberts, W. M. 1993. Spatial calcium buffering in saccular hair cells. *Nature.* 363:74–76.
- Roberts, W. M. 1994. Localization of calcium signals by a mobile calcium buffer in frog saccular hair cells. *J. Neurosci.* 14:3246–3262.
- Robitaille, R., and M. P. Charlton. 1991. Frequency facilitation is not caused by residual ionized calcium at the frog neuromuscular junction. *Ann. N. Y. Acad. Sci.* 635:492–494.
- Rozov, A., N. Burnashev, B. Sakmann, and E. Neher. 2001. Transmitter release modulation by intracellular  $\text{Ca}^{2+}$  buffers in facilitating and depressing nerve terminals of pyramidal cells in layer 2/3 of the rat neocortex indicates a target cell-specific difference in presynaptic calcium dynamics. *J. Physiol.* 531:807–826.
- Sala, F., and A. Hernández-Cruz. 1990. Calcium diffusion modeling in a spherical neuron. Relevance of buffering properties. *Biophys. J.* 57: 313–324.
- Sätzler, K., L. F. Sohl, J. H. Bollmann, J. G. Borst, M. Frotscher, B. Sakmann, and J. H. Lubke. 2002. Three-dimensional reconstruction of a calyx of Held and its postsynaptic principal neuron in the medial nucleus of the trapezoid body. *J. Neurosci.* 22:10567–10579.
- Schneggenburger, R., and E. Neher. 2000. Intracellular calcium dependence of transmitter release rates at a fast central synapse. *Nature.* 406:889–893.
- Sheng, Z. H., R. E. Westenbroek, and W. A. Catterall. 1998. Physical link and functional coupling of presynaptic calcium channels and the synaptic vesicle docking/fusion machinery. *J. Bioenerg. Biomembr.* 30:335–345.
- Simon, S. M., and R. R. Llinás. 1985. Compartmentalization of the submembrane calcium activity during calcium influx and its significance in transmitter release. *Biophys. J.* 48:485–498.
- Smith, G. D., L.-X. Dai, R. Miura, and A. Sherman. 2001. Asymptotic analysis of equations for the buffered diffusion of intracellular calcium. *SIAM J. Applied Math.* 61:1816–1838.
- Smith, G. D., J. Wagner, and J. Keizer. 1996. Validity of the rapid buffering approximation near a point source of calcium ions. *Biophys. J.* 70:2527–2539.
- Stanley, E. F. 1997. The calcium channel and the organization of the presynaptic transmitter release face. *Trends Neurosci.* 20:404–409.

- Tang, Y., T. Schlumpberger, T. Kim, M. Lueker, and R. S. Zucker. 2000. Effects of mobile buffers on facilitation: experimental and computational studies. *Biophys. J.* 78:2735–2751.
- Tank, D. W., W. G. Regehr, and K. R. Delaney. 1995. A quantitative analysis of presynaptic calcium dynamics that contribute to short-term enhancement. *J. Neurosci.* 15:7940–7952.
- Trommershäuser, J., R. Schneggenburger, A. Zippelius, and E. Neher. 2003. Heterogeneous presynaptic release probabilities: functional relevance for short-term plasticity. *Biophys. J.* 84:1563–1579.
- Vyshedskiy, A., and J.-W. Lin. 1997. Activation and detection of facilitation as studied by presynaptic voltage control at the inhibitor of the crayfish opener muscle. *J. Neurophysiol.* 77:2300–2315.
- Vyshedskiy, A., and J.-W. Lin. 2000. Presynaptic  $\text{Ca}^{2+}$  influx at the inhibitor of the crayfish neuromuscular junction: a photometric study at a high time resolution. *J. Neurophysiol.* 83:552–562.
- Winslow, J. L., S. N. Duffy, and M. P. Charlton. 1994. Homosynaptic facilitation of transmitter release in crayfish is not affected by mobile calcium chelators: implications for the residual ionized calcium hypothesis from electrophysiological and computational analyses. *J. Neurophysiol.* 72:1769–1793.
- Wright, S. N., M. S. Brodwick, and G. D. Bittner. 1996. Calcium currents, transmitter release and facilitation of release at voltage-clamped crayfish nerve terminals. *J. Physiol.* 496:363–378.
- Xu, T., M. Naraghi, H. Kang, and E. Neher. 1997. Kinetic studies of  $\text{Ca}^{2+}$  binding and  $\text{Ca}^{2+}$  clearance in the cytosol of adrenal chromaffin cells. *Biophys. J.* 73:532–545.
- Yamada, W. M., and R. S. Zucker. 1992. Time course of transmitter release calculated from simulations of a calcium diffusion model. *Biophys. J.* 61:671–682.
- Zhou, Z., and E. Neher. 1993. Mobile and immobile calcium buffers in bovine adrenal chromaffin cells. *J. Physiol.* 469:245–273.
- Zucker, R. S. 1974. Characteristics of crayfish neuromuscular facilitation and their calcium dependence. *J. Physiol.* 241:91–110.
- Zucker, R. S. 1994. Calcium and short-term synaptic plasticity. *Neth. J. Zool.* 44:495–512.
- Zucker, R. S. 1996. Exocytosis: a molecular and physiological perspective. *Neuron.* 17:1049–1055.
- Zucker, R. S. 1999. Calcium- and activity-dependent synaptic plasticity. *Curr. Opin. Neurobiol.* 9:305–313.
- Zucker, R. S., and W. G. Regehr. 2002. Short-term synaptic plasticity. *Annu. Rev. Physiol.* 64:355–405.